ACADEMIC PRESS

Available online at www.sciencedirect.com

SCIENCE DIRECT®

Journal of Sound and Vibration 262 (2003) 921–975

JOURNAL OF SOUND AND VIBRATION

www.elsevier.com/locate/jsvi

Theory and experiments for large-amplitude vibrations of empty and fluid-filled circular cylindrical shells with imperfections

M. Amabili*

Dipartimento di Ingegneria Industriale, Università di Parma, Parco Area delle Scienze 181/A, 43100 Parma, Italy

Received 8 November 2001; accepted 20 February 2002

Abstract

The large-amplitude response of perfect and imperfect, simply supported circular cylindrical shells to harmonic excitation in the spectral neighbourhood of some of the lowest natural frequencies is investigated. Donnell's non-linear shallow-shell theory is used and the solution is obtained by the Galerkin method. Several expansions involving 16 or more natural modes of the shell are used. The boundary conditions on the radial displacement and the continuity of circumferential displacement are exactly satisfied. The effect of internal quiescent, incompressible and inviscid fluid is investigated. The non-linear equations of motion are studied by using a code based on the arclength continuation method. A series of accurate experiments on forced vibrations of an empty and water-filled stainless-steel shell have been performed. Several modes have been intensively investigated for different vibration amplitudes. A closed loop control of the force excitation has been used. The actual geometry of the test shell has been measured and the geometric imperfections have been introduced in the theoretical model. Several interesting non-linear phenomena have been experimentally observed and numerically reproduced, such as softening-type non-linearity, different types of travelling wave response in the proximity of resonances, interaction among modes with different numbers of circumferential waves and amplitude-modulated response. For all the modes investigated, the theoretical and experimental results are in strong agreement.

1. Introduction

Large-amplitude vibrations of circular cylindrical shells have interested many researchers in the second half of the last century. However, experimental results are still scarce and the effect of geometric imperfections still needs clarification.

*Tel.: +39-0521-905-896; fax: +39-0521-905-705.
E-mail address: marco@me.unipr.it (M. Amabili).
URL: http://me.unipr.it/mam/amabili/amabili.html.

0022-460X/03/$ - see front matter
PII: S0022-460X(02)01051-9

A full literature review of work on the non-linear dynamics of shells in vacuo, filled with or surrounded by quiescent and flowing fluids has been given by Amabili and Païdoussis [1] and will not be repeated here. However, it is necessary to refer to some fundamental and some recent contributions. Briefly, it is possible to attribute to Evensen [2] and Dowell and Ventres [3] the original idea of mode expansions of the shell flexural displacement involving the two asymmetric modes with the same shape (sine and cosine functions around the shell circumference; one is directly driven by external excitation, the driven mode; the other is referred to as the companion mode) and an axisymmetric term; their intuition was supported by a few available experimental results. The studies of Ginsberg [4] and Chen and Babcock [5] constitute important contributions to the study of the influence of the companion mode on the non-linear forced response of circular cylindrical shells. Ganapathi and Varadan [6] studied the free response by using the finite element method. Gonçalves and Batista [7] and Amabili et al. [8] studied the response of fluid-filled shells. In particular, Gonçalves and Batista [7] neglected companion mode participation, the importance of which in the non-linear response was investigated by Amabili et al. [8]. In a recent series of papers Amabili et al. [9–13] systematically studied the non-linear dynamics and large-amplitude vibrations of circular cylindrical shells with and without quiescent or flowing fluid by using a base of seven natural modes. The convergence of the solution was recently studied by Pellicano et al. [14] by using additional modes; a parametric study was also performed to investigate switches for softening type to hardening type non-linearity.

Geometric imperfections of the shell geometry (out-of-roundness) were considered in buckling problems since the end of the 1950s. However, there is no trace of their inclusion in studies of large-amplitude vibrations of shells until the beginning of the 1970s. Research on this topic was probably introduced by Vol'mir [15]. Kubenko et al. [16] used a two-mode travelling-wave expansion, taking into account axisymmetric and asymmetric geometric imperfections. Only free vibrations were studied, but the effect of the number of circumferential waves on the non-linearity was investigated. In particular, the results showed that the non-linearity is of softening type and that it increases with the number of circumferential waves. The effect of axisymmetric and asymmetric imperfections was to increase the value of the natural frequency; this is in contrast with results of other studies.

Watawala and Nash [17] studied the free and forced conservative vibrations of closed circular cylindrical shells by using Donnell's non-linear shallow-shell theory. Empty and liquid-filled shells with a free-surface and a rigid bottom were studied. A mode expansion that may be considered a simple generalization of Evensen's [2] was introduced; it implies a no moment-free condition at both ends of the shell. A single term was used to describe shell geometric imperfections. Cases of (i) the mode shape of the shell response being the same as that of the imperfections and (ii) the mode shape of the response being different (actually the same, but rotated) from that of the imperfections were analyzed. Numerical results showed softening type non-linearity. The imperfections lowered the linear frequency of vibrations when the mode shape of the shell response is the same as that of the imperfection, and they affected the non-linearity. Results for forced vibrations were obtained only for beam-bending modes, for which Donnell's non-linear shallow-shell theory is not appropriate; these results indicated hardening type non-linearity.

Amabili and Pellicano [18] studied non-linear supersonic flutter of imperfect circular shells by using Donnell's non-linear shallow-shell theory and expansions with up to 22 modes. They

introduced asymmetric and axisymmetric geometric imperfections expanded in a series of seven terms.

Experimental work is much less abundant than theoretical and numerical study. Chen and Babcock [5] measured the softening type response for the fundamental mode of an empty shell with end rings and detected travelling waves around the shell at an excitation frequency close to a resonance. Sivak and Telalov [19] obtained experimental results for the backbone curve (relative to free vibrations) on a vertical circular cylindrical shell made of titanium alloy in contact with water having a free surface. Experiments were performed with the shell partially filled and partially submerged in water, under radial excitation. The experimental boundary conditions simulated a clamped shell. Most of the experiments indicated softening-type non-linearity. Chiba [20,21] experimentally studied large-amplitude vibrations of two vertical cantilevered circular cylindrical shells made of polyester sheet, empty and partially filled with water to different levels. He observed that for modes with the same axial wavenumber, the weakest non-linearity (as usual, of the softening type) is associated to the mode having the minimum natural frequency. He also found that shorter tanks have a larger softening non-linearity than longer ones. The tank with a lower liquid height had a greater softening non-linearity than the tank with a higher liquid level. Travelling wave response and coupling between two bulging modes (and between two sloshing modes) were also observed. Large-amplitude vibrations of two vertical clamped circular cylindrical shells, partially filled with water to different levels were also studied by Chiba [22]. Amabili et al. [23] have given the details on the experiments reported in Ref. [11] for comparison purpose. The softening response was measured but the travelling wave was not observed for asymmetry of the test shell and added masses of sensors.

Non-linear interaction between asymmetric and axisymmetric modes has been investigated by Amabili et al. [24] and Pellicano et al. [25] in case of internal resonances. Interaction between asymmetric modes with different number of circumferential waves has been studied by Kubenko and Koval'chuk [26].

The present paper extends the study of Amabili et al. [11] (i) to deal with shells having geometric imperfections, (ii) using very accurate mode expansions (16 or more modes instead of 7), which permit one to reach convergence of the solution as shown in Ref. [14], and (iii) presenting, discussing and reproducing numerically a new series of accurate and complete experimental results on an empty and water-filled shell. The response of simply supported circular cylindrical shells to harmonic excitation in the spectral neighbourhood of some of the lowest natural frequencies is investigated in this paper. Donnell's non-linear shallow-shell theory is used and the solution is obtained by Galerkin projection. Experiments on an empty and water-filled circular cylindrical shell made of stainless steel have given results in good agreement with the present theory. The imposed boundary conditions approximate a simply supported shell at both ends.

2. Equation of motion, boundary conditions and mode expansion

A cylindrical co-ordinate system $(O; x, r, \theta)$ is chosen, with the origin O placed at the centre of one end of the shell. The displacements of points in the middle surface of the shell are denoted by u, v and w, in the axial, circumferential and radial directions, respectively; w is taken positive

inwards. Initial imperfections of the circular cylindrical shell associated with zero initial tension are denoted by inward radial displacement w_0; only radial initial imperfections are considered. By using Donnell's non-linear shallow-shell theory, the equation of motion for finite-amplitude transverse dynamic deformation of a thin, imperfect, circular cylindrical shell is given by [17,18]

$$D\nabla^4 w + ch\dot{w} + \rho h\ddot{w} = f - p + \frac{1}{R}\frac{\partial^2 F}{\partial x^2} + \frac{1}{R^2}\left[\frac{\partial^2 F}{\partial \theta^2}\left(\frac{\partial^2 w}{\partial x^2} + \frac{\partial^2 w_0}{\partial x^2}\right) - 2\frac{\partial^2 F}{\partial x \partial \theta}\left(\frac{\partial^2 w}{\partial x \partial \theta} + \frac{\partial^2 w_0}{\partial x \partial \theta}\right) + \frac{\partial^2 F}{\partial x^2}\left(\frac{\partial^2 w}{\partial \theta^2} + \frac{\partial^2 w_0}{\partial \theta^2}\right)\right], \tag{1}$$

where $D = Eh^3/[12(1-\nu^2)]$ is the flexural rigidity, E Young's modulus, ν the Poisson ratio, h the shell thickness, R the mean shell radius, ρ the mass density of the shell, c the coefficient of viscous damping, p the radial pressure applied to the surface of the shell as a consequence of the contained fluid, and f is an external modal excitation of unspecified physical origin, which has the form

$$f = f_{1,n}\cos(n\theta)\sin(\pi x/L)\cos(\omega t), \tag{2}$$

where $f_{1,n}$ is a coefficient having dimension of pressure. Excitations with frequency close to the natural frequency of lowest modes are considered; low-frequency modes have a predominant radial motion and are identified by the pair (n, m), where n is the number of circumferential waves and m is the number of axial half-waves. The viscous damping model introduced in Eq. (1) is unrealistic and will be replaced by modal-damping coefficients experimentally identified in the equations of motion used to perform numerical calculations.

In Eq. (1) the overdot denotes a time derivative and F is the in-plane Airy stress function. Here F is given by the following compatibility equation [17,18]:

$$\frac{1}{Eh}\nabla^4 F = -\frac{1}{R}\frac{\partial^2 w}{\partial x^2} + \frac{1}{R^2}\left[\left(\frac{\partial^2 w}{\partial x \partial \theta}\right)^2 + 2\frac{\partial^2 w}{\partial x \partial \theta}\frac{\partial^2 w_0}{\partial x \partial \theta} - \left(\frac{\partial^2 w}{\partial x^2} + \frac{\partial^2 w_0}{\partial x^2}\right)\frac{\partial^2 w}{\partial \theta^2} - \frac{\partial^2 w}{\partial x^2}\frac{\partial^2 w_0}{\partial \theta^2}\right]. \tag{3}$$

In Eqs. (1) and (3), the biharmonic operator is defined as $\nabla^4 = [\partial^2/\partial x^2 + \partial^2/(R^2\partial\theta^2)]^2$. Donnell's non-linear shallow-shell equations are accurate only for modes with a large number n of circumferential waves; specifically, $1/n^2 \ll 1$ is required in order to have fairly good accuracy (i.e., $n \geqslant 4$ or 5). Donnell's non-linear shallow-shell equations are obtained by neglecting the in-plane inertia, transverse shear deformation and rotary inertia, giving accurate results only for very thin shells, i.e., $h \ll R$. In-plane displacements are assumed to be infinitesimal, i.e., $|u| \ll h, |v| \ll h$, whereas w is of the same order of the shell thickness.

The forces per unit length in the axial and circumferential directions, as well as the shear force, are given by [3]

$$N_x = \frac{1}{R^2}\frac{\partial^2 F}{\partial \theta^2}, \qquad N_\theta = \frac{\partial^2 F}{\partial x^2}, \qquad N_{x\theta} = -\frac{1}{R}\frac{\partial^2 F}{\partial x \partial \theta}. \tag{4}$$

The force–displacement relations are

$$(1-\nu^2)\frac{N_x}{Eh} = -\frac{\nu w}{R} + \frac{1}{2}\left(\frac{\partial w}{\partial x}\right)^2 + \frac{\partial w}{\partial x}\frac{\partial w_0}{\partial x} + \frac{\nu}{2}\left(\frac{\partial w}{R\partial \theta}\right)^2 + \nu\frac{\partial w}{R\partial \theta}\frac{\partial w_0}{R\partial \theta} + \frac{\partial u}{\partial x} + \frac{\nu}{R}\frac{\partial v}{\partial \theta}, \tag{5}$$

$$(1-\nu^2)\frac{N_\theta}{Eh} = -\frac{w}{R} + \frac{\nu}{2}\left(\frac{\partial w}{\partial x}\right)^2 + \nu\frac{\partial w}{\partial x}\frac{\partial w_0}{\partial x} + \frac{1}{2}\left(\frac{\partial w}{R\partial\theta}\right)^2 + \frac{\partial w}{R\partial\theta}\frac{\partial w_0}{R\partial\theta} + \nu\frac{\partial u}{\partial x} + \frac{1}{R}\frac{\partial v}{\partial\theta}, \tag{6}$$

$$(1-\nu^2)\frac{N_{x\theta}}{Eh} = 2(1-\nu)\left[\frac{1}{R}\frac{\partial w}{\partial x}\frac{\partial w}{\partial\theta} + \frac{1}{R}\frac{\partial w}{\partial x}\frac{\partial w_0}{\partial\theta} + \frac{1}{R}\frac{\partial w_0}{\partial x}\frac{\partial w}{\partial\theta} + \frac{1}{R}\frac{\partial u}{\partial\theta} + \frac{\partial v}{\partial x}\right]. \tag{7}$$

In this study, attention is focused on a finite, simply supported, circumferentially closed circular cylindrical shell of length L. The following out-of-plane boundary conditions are imposed:

$$w = w_0 = 0, \tag{8a}$$

$$M_x = -D\{(\partial^2 w/\partial x^2) + \nu[\partial^2 w/(R^2\partial\theta^2)]\} = 0, \tag{8b}$$

$$\partial^2 w_0/\partial x^2 = 0 \quad \text{at } x = 0, L, \tag{8c}$$

where M_x is the bending moment per unit length. The in-plane boundary conditions are

$$N_x = 0 \quad \text{at } x = 0, L. \tag{9a}$$

and

$$v = 0 \quad \text{at } x = 0, L. \tag{9b}$$

Moreover, u, v and w must be continuous in θ.

Past studies show that a linear modal base is the simplest choice to discretize the system. In particular, in order to reduce the number of degrees of freedom, it is important to use only the most significant modes. It is necessary to consider, in addition to the asymmetric mode directly driven into vibration by the excitation (driven mode), (i) the orthogonal mode having the same shape and natural frequency but rotated by $\pi/(2n)$ (companion mode), (ii) additional asymmetric modes, and (iii) axisymmetric modes. In fact, it has clearly been established that, for large-amplitude shell vibrations, the deformation of the shell involves significant axisymmetric oscillations inwards (see Section 8.3). According to these considerations, the radial displacement w is expanded by using the eigenmodes of the empty shell (which are unchanged for the completely filled shell):

$$w(x,\theta,t) = \sum_{m=1}^{M_1}\sum_{n=1}^{N}[A_{m,n}(t)\cos(n\theta) + B_{m,n}(t)\sin(n\theta)]\sin(\lambda_m x) + \sum_{m=1}^{M_2} A_{m,0}(t)\sin(\lambda_m x), \tag{11a}$$

where n is the number of circumferential waves, m is the number of longitudinal half-waves, $\lambda_m = m\pi/L$ and t is the time, $A_{m,n}(t)$, $B_{m,n}(t)$ and $A_{m,0}(t)$ are the generalized co-ordinates that are unknown functions of t. The integers N, M_1 and M_2 must be selected with care in order to obtain the required accuracy and acceptable dimension of the non-linear problem. The number of degrees of freedom used in the present numerical calculations is 16 or more. It is observed, for symmetry reasons, that the non-linear interaction among linear modes of the chosen base involves the asymmetric modes ($n > 0$) having a given n value (the resonant mode), the asymmetric modes having a multiple of this value of circumferential waves ($k \times n$, where k is an integer), and axisymmetric modes ($n = 0$); asymmetric modes with different numbers of circumferential waves, that do not satisfy the relationship $k \times n$, have interaction only if their natural frequencies are very

close to relationship 1:1, 1:2 or 1:3 with the frequency of the resonant mode (n, m). Only modes with an odd m value of longitudinal half-waves can be considered for symmetry reasons [8,9,11] (if imperfections with an even m value are not introduced). In particular, asymmetric modes having up to three longitudinal half-waves ($M_1 = 3$, only odd m values) and modes having n, $2 \times n$ and $3 \times n$ circumferential waves have been considered in the numerical calculations. For axisymmetric modes $M_2 = 7$ has been used (only odd m values). Actually, $M_1 = M_2 = 3$ is sufficient to guarantee good accuracy. However, as it has been shown in Refs. [11,14], additional axisymmetric modes give a small contribution to the shell response while additional asymmetric modes with more than three longitudinal half-waves are practically negligible. This is the reason for having M_2 larger than M_1. The form of the radial displacement used in the numerical calculation is

$$w(x,\theta,t) = \sum_{m=1}^{3}\sum_{k=1}^{3}[A_{m,kn}(t)\cos(kn\theta) + B_{m,kn}(t)\sin(kn\theta)]\sin(\lambda_m x) + \sum_{m=1}^{4} A_{(2m-1),0}(t)\sin(\lambda_{(2m-1)}x). \tag{11b}$$

However, expansions involving additional asymmetric modes that do not satisfy the relationship $k \times n$, but having frequency close to relationship 1:1 or 1:2 with the driven mode, have been introduced for some cases (see Sections 8.2 and 8.3).

The presence of couples of modes having the same shape but different angular orientations, the first one described by $\cos(n\,\theta)$ (driven mode for the excitation given by Eq. (2)) and the other by $\sin(n\,\theta)$ (companion mode), in the periodic response of the shell leads to the appearance of travelling-wave vibration around the shell in the angular direction (see Section 4.1). This phenomenon is related to the axial symmetry of the system.

When the excitation has a frequency close to the resonance of mode $(n, m = 1)$, results show that the generalized co-ordinates $A_{1,n}(t)$ and $B_{1,n}(t)$ have the same frequency as that of the excitation; the co-ordinates $A_{1,2n}(t)$, $B_{1,2n}(t)$, $A_{3,2n}(t)$, $B_{3,2n}(t)$ and all the co-ordinates associated to axisymmetric modes have twice the frequency of the excitation; the co-ordinates $A_{3,n}(t)$, $B_{3,n}(t)$, $A_{1,3n}(t)$, $B_{1,3n}(t)$, $A_{3,3n}(t)$ and $B_{3,3n}(t)$ have three times the frequency of the excitation.

The initial radial imperfection w_0 is expanded in the same form of w, i.e., in a double Fourier series satisfying boundary conditions (8a) and (8c) at the shell edges,

$$w_0(x,\theta) = \sum_{m=1}^{\tilde{M}_1}\sum_{n=1}^{\tilde{N}}[\tilde{A}_{m,n}\cos(n\theta) + \tilde{B}_{m,n}\sin(n\theta)]\sin(\lambda_m x) + \sum_{m=1}^{\tilde{M}_2}\tilde{A}_{m,0}\sin(\lambda_m x), \tag{12}$$

where $\tilde{A}_{m,n}$, $\tilde{B}_{m,n}$ and $\tilde{A}_{m,0}$ are the modal amplitudes of imperfections; $\tilde{N}$, $\tilde{M}_1$ and $\tilde{M}_2$ are integers indicating the number of terms in the expansion.

3. Fluid–structure interaction

The contained fluid is assumed to be incompressible and inviscid. Liquid-filled shells vibrating in low-frequency range satisfy very well the incompressible hypothesis. The non-linear effects in

the dynamic pressure and in the boundary conditions at the fluid–structure interface are neglected. These non-linear effects have been found to be negligible by Gonçalves and Batista [7] and Lakis and Laveau [27]. The shell prestress due to the fluid weight is also neglected. The fluid motion is described by the velocity potential Φ, which satisfies the Laplace equation

$$\nabla^2\Phi = \frac{\partial^2\Phi}{\partial x^2} + \frac{\partial^2\Phi}{\partial r^2} + \frac{1}{r}\frac{\partial\Phi}{\partial r} + \frac{1}{r^2}\frac{\partial^2\Phi}{\partial\theta^2} = 0. \tag{13}$$

The velocity of the fluid is related to Φ by $\mathbf{v} = -\nabla\Phi$. No cavitation is assumed at the fluid-shell interface,

$$\left(\frac{\partial\Phi}{\partial r}\right)_{r=R} = \dot{w}. \tag{14}$$

Both ends of the fluid volume (in correspondence to the shell edges) are assumed to be open, so that a zero pressure is assumed there,

$$(\Phi)_{x=0} = (\Phi)_{x=L} = 0. \tag{15}$$

A solution of Eq. (13) satisfying condition (15) is given by

$$\Phi = \sum_{m=1}^{\infty}\sum_{n=0}^{\infty}[\alpha_{mn}(t)\cos(n\theta) + \beta_{mn}(t)\sin(n\theta)]\,[c_{mn}\mathrm{I}_n(\lambda_m r) + d_{mn}\mathrm{K}_n(\lambda_m r)]\sin(\lambda_m x), \tag{16}$$

where $\mathrm{I}_n(r)$ and $\mathrm{K}_n(r)$ are the modified Bessel functions of the first and second kind of order n, respectively. Eq. (16) must satisfy boundary condition (14) and Φ must be finite (regular) at $r = 0$. By using the assumed mode shapes w, given by Eq. (11), the solution of the boundary-value problem for internal fluid only is

$$\Phi = \sum_{m=1}^{M}\sum_{n=0}^{N}[\dot{A}_{mn}(t)\cos(n\theta) + \dot{B}_{mn}(t)\sin(n\theta)]\frac{\mathrm{I}_n(\lambda_m r)}{\lambda_m \mathrm{I}'_n(\lambda_m R)}\sin(\lambda_m x), \tag{17}$$

where $\mathrm{I}'_n(r)$ is the derivative of $\mathrm{I}_n(r)$ with respect to its argument and M is the largest between M_1 and M_2. Therefore, the dynamic pressure p exerted by the contained fluid on the shell is given by

$$p = \rho_F(\dot{\Phi})_{r=R} = \sum_{m=1}^{M}\sum_{n=0}^{N}\rho_F[\ddot{A}_{mn}(t)\cos(n\theta) + \ddot{B}_{mn}(t)\sin(n\theta)]\frac{\mathrm{I}_n(\lambda_m R)}{\lambda_m \mathrm{I}'_n(\lambda_m R)}\sin(\lambda_m x), \tag{18}$$

where ρ_F is the mass density of the internal fluid. Eq. (18) shows that the inertial effects due to the fluid are different for the asymmetric and the axisymmetric terms of the mode expansion. Hence, the fluid is expected to change the non-linear behaviour of the fluid-filled shell. Usually the inertial effect of the fluid is larger for axisymmetric modes, thus enhancing the non-linear behaviour of the shell (see Section 8.2).

4. Stress function and solution

Expansions (11a) and (11b) used for the radial displacement w satisfy identically the boundary conditions given by Eqs. (8a) and (8b); moreover, they satisfy exactly the continuity of the

circumferential displacement [8],

$$\int_0^{2\pi} \partial v/\partial\theta \, \mathrm{d}\theta = v(2\pi) - v(0) = 0, \tag{19}$$

as has been verified after calculation of the stress function F from Eq. (3).

The boundary conditions for the in-plane displacements, Eqs. (9a) and (9b), give very complex expressions when transformed into equations involving w. Therefore, they are modified into simpler integral expressions that satisfy Eqs. (9a) and (9b) on the average [3]. Specifically, the following conditions are imposed:

$$\int_0^{2\pi} N_x R \, \mathrm{d}\theta = 0, \quad \text{at } x = 0, L, \tag{20}$$

$$\int_0^{2\pi} \int_0^{L} N_{x\theta} \, \mathrm{d}x \, R \, \mathrm{d}\theta = 0. \tag{21}$$

Eq. (20) ensures a zero axial force N_x on the average at $x = 0, L$; Eq. (21) is satisfied when $v = 0$ on the average at $x = 0$, L and u is continuous in θ on the average. Substitution of Eqs. (9a) and (9b) into Eqs. (20) and (21) simplifies computations, although it introduces an approximation (boundary conditions (9a) and (9b) are exactly satisfied at n discrete points, where n is the number of circumferential waves).

When the expansions of w and w_0, Eqs. (11a) and (12), are substituted in the right-hand side of Eq. (3), a partial differential equation for the stress function F is obtained; the solution may be written as

$$F = F_h + F_p, \tag{22}$$

where F_h is the homogeneous solution and F_p the particular solution. The particular solution is given by

$$\begin{aligned} F_p = &\sum_{m=1}^{2M}\sum_{n=1}^{2N}(F_{mn1}\sin m\eta \sin n\theta + F_{mn2}\sin m\eta \cos n\theta + F_{mn3}\cos m\eta \sin n\theta + F_{mn4}\cos m\eta \cos n\theta) \\ &+ \sum_{n=1}^{2N}(F_{0n3}\sin n\theta + F_{mn4}\cos n\theta) + \sum_{m=1}^{2M}(F_{m02}\sin m\eta + F_{m04}\cos m\eta), \end{aligned} \tag{23}$$

where N is the same as in Eq. (11a), M is the largest between M_1 and M_2, $\eta = \pi x/L$ and the functions of time F_{mnj}, $j = 1, \ldots, 4$, have a long expression not reported here; they have been identified by using the *Mathematica* computer program [28] for symbolic manipulations by using the technique sited in Appendix A. The homogeneous solution may be assumed to have the form [8,9]

$$F_h = \frac{1}{2}\bar{N}_x R^2\theta^2 + \frac{1}{2}x^2\left\{\bar{N}_\theta - \frac{1}{2\pi RL}\int_0^{L}\int_0^{2\pi}\left[\frac{\partial^2 F_p}{\partial x^2}\right] R \, \mathrm{d}\theta \, \mathrm{d}x\right\} - \bar{N}_{x\theta} x R\theta, \tag{24}$$

where $\bar{N}_x$, $\bar{N}_\theta$, and $\bar{N}_{x\theta}$ are the average in-plane restraint stresses (forces per unit length) generated at the shell ends, defined as

$$\bar{N}_\# = [1/(2\pi L)] \int_0^{2\pi} \int_0^L N_\# \, \mathrm{d}x \, \mathrm{d}\theta, \tag{25}$$

where the symbol # must be replaced by x, θ and $x\theta$. Boundary conditions (20) and (21) allow one to express $\bar{N}_x$, $\bar{N}_\theta$ and $\bar{N}_{x\theta}$, see Eqs. (5)–(7), in terms of w, w_0 and their derivatives. The expressions obtained inserting the expansion of w given by Eq. (11b) in Eqs. (5)–(7) and (25) are given in Appendix B. Eq. (24) is chosen in order to satisfy the boundary conditions imposed. Moreover, it satisfies Eqs. (4) on the average.

By use of the Galerkin method, 16 (or more) second order, ordinary, coupled non-linear differential equations are obtained for the variables $A_{m,kn}(t)$, $B_{m,kn}(t)$ and $A_{m,0}(t)$, for $m = 1, \ldots, M$ and $k = 1, \ldots, 3$, by successively weighting the single original Eq. (1) with the functions that describe the shape of the modes retained in Eq. (11). These equations have very long expressions containing quadratic and cubic non-linear terms and are studied both by using (i) the software AUTO 97 [29] for continuation and bifurcation analysis of non-linear ordinary differential equations, and (ii) direct integration of the equations of motion by using the DIVPAG routine of the program library IMSL. The software AUTO 97 is capable of continuation of the solution, bifurcation analysis and branch switching by using arclength continuation and collocation methods. In particular, the shell response under harmonic excitation has been studied by using an analysis in two steps: (i) first the excitation frequency has been fixed far enough from resonance and the magnitude of the excitation has been used as bifurcation parameter; the solution has been started at zero force where the solution is the trivial undisturbed configuration of the shell and has been continued up to reach the desired force magnitude; (ii) when the desired magnitude of excitation has been reached, the solution has been continued by using the excitation frequency as bifurcation parameter.

The Galerkin projections of the equation of motion (1) have been performed analytically by using the *Mathematica* computer software [28] in order to avoid numerical errors, which arise from numerical calculations of surface integrals of trigonometric functions. The Galerkin projection of the modal excitation f on the weighting functions z_s, gives

$$\langle f, z_s \rangle = \int_0^{2\pi} \int_0^L f z_s \, \mathrm{d}x \, R \mathrm{d}\theta = \begin{cases} \dfrac{\pi R L}{2} f_{1,n} \cos(\omega t) & \text{for } s = 1, \\ 0 & \text{for } s \neq 1, \end{cases} \tag{26}$$

where $z_1 = \cos(n\theta)\sin(\pi x/L)$, $z_2 = \sin(n\theta)\sin(\pi x/L)$, … according to the mode expansion utilized. Therefore, the modal excitation considered gives a non-zero contribution only to mode $A_{1,n}(t)\cos(n\theta)\sin(\pi x/L)$, i.e., on the driven mode. The mode having the shape of the driven mode, but rotated by $\pi/(2n)$, i.e., with form $B_{1,n}(t)\sin(n\theta)\sin(\pi x/L)$, is referred to as the companion mode and is not directly excited in this case.

This kind of external excitation is quite unrealistic. Practically, one or more forces are usually applied to the system. A more realistic case is the one of a harmonic point excitation, modelling for instance the excitation by an electro-dynamical exciter (shaker); the above considerations are important in the analysis of the experimental results presented in Sections 7 and 8. The point force

excitation $\tilde{f}$ is the resultant of the pressure distribution

$$f = \tilde{f}\delta(R\theta - R\tilde{\theta})\delta(x - \tilde{x})\cos(\omega t), \tag{27}$$

where δ is the Dirac delta function, $\tilde{f}$ is the magnitude of the localized force, $\tilde{\theta}$ and $\tilde{x}$ give the angular and axial co-ordinates of the point of application of the force, respectively. If the point excitation is located at $\tilde{\theta} = 0$, $\tilde{x} = L/2$, the Galerkin projection of the excitation f on the weighing functions z_s gives

$$\langle f, z_s \rangle = \begin{cases} \tilde{f}\cos(\omega t) & \text{for } z_s \text{ axisymmetric or containing } \cos(n\theta), \\ 0 & \text{for } z_s \text{ containing } \sin(n\theta). \end{cases} \tag{28}$$

In this case, setting $\tilde{f} = f_{1,n}\pi RL/2$ the only difference between modal excitation and point excitation is that the point excitation directly drives all modes described by a cosine function in angular direction θ and also the axisymmetric modes.

4.1. Travelling wave response

Away from resonance, the companion mode solution disappears ($B_{1,n}(t) = 0$) and the generalized co-ordinates are nearly in phase or in opposite phase. The presence of the companion mode in the shell response leads to the appearance of a travelling wave and to more complex phase relationships among the generalized co-ordinates. The flexural mode shapes are represented by Eq. (11). Upon supposing that the response of the driven and companion modes have the same frequency of oscillation, i.e., $A_{1,n}(t) = a_{1,n}\cos(\omega t + \theta_1)$ and $B_{1,n}(t) = b_{1,n}\cos(\omega t + \theta_2)$, and considering the other co-ordinates having smaller amplitude, Eq. (11) can be rearranged as

$$\begin{aligned} w = {} & \{[a_{1,n}\cos(\omega t + \theta_1) + b_{1,n}\sin(\omega t + \theta_2)]\cos(n\theta) + b_{1,n}\sin(n\theta - \omega t - \theta_2)\}\sin(\pi x/L) \\ & + O(a_{1,n}^2, b_{1,n}^2, a_{3,n}, \ldots, a_{1,0}, a_{3,0}, \ldots), \end{aligned} \tag{29}$$

where $a_{1,n}$ and $b_{1,n}$ are the amplitudes of driven and companion modes, respectively, and θ_1 and θ_2 are the phases. Eq. (29) gives a combined solution consisting of a standing wave plus a travelling wave of amplitude $b_{1,n}$ moving in angular direction around the shell with angular velocity ω/n. The resulting standing wave is given by the sum of the two standing waves, one of amplitude $a_{1,n}$ and the second of amplitude $b_{1,n}$, having the same circular frequency ω and the same shape, but having a phase difference of $\theta_2 - \theta_1 - \pi/2$. When $\theta_2 - \theta_1 \cong \pi/2$, as it is generally observed in calculations and experiments, the amplitude of the resulting standing wave is almost $a_{1,n} - b_{1,n}$; therefore it becomes zero for $a_{1,n} = b_{1,n}$ and $\theta_2 - \theta_1 = \pi/2$, when a pure travelling wave appears. The amplitude and frequency of the travelling wave solution are not affected by the phase relationship between driven and companion modes.

It is important to observe that the companion mode arises as a consequence of the symmetry of the system. This phenomenon represents a fundamental difference vis-à-vis linear vibrations.

5. Experimental set-up

Tests have been conducted on a commercial circular cylindrical shell made of stainless steel and having a longitudinal seam weld. The dimensions and material properties of the shell are:

$L = 520\,\text{mm}$, $R = 149.4\,\text{mm}$, $h = 0.519\,\text{mm}$, $E = 1.98 \times 10^{11}\,\text{Pa}$, $\rho = 7800\,\text{kg/m}^3$, $\rho_F = 1000\,\text{kg/m}^3$ and $\nu = 0.3$. Two stainless-teel annular plates of external and internal radius of 149.4 and 60 mm, respectively, and thickness 0.25 mm have been welded to the shell ends to approximate the simply supported boundary condition of the shell. A rubber disk 1 mm thick has been glued to each of these annular end plates (see Fig. 1). The tank has been tested empty and completely filled with water. The zero pressure boundary condition is well approximated by the flexible rubber disks at the shell ends. Two small pipe fittings were welded onto one of the end plates in such a position that they do not affect shell vibrations; they are used for filling the specimen with water.

The shell has been suspended horizontally with cables to a box-type frame and has been subjected to (i) burst-random excitation to identify the natural frequencies and perform a modal analysis by measuring the shell response on a grid of points, (ii) harmonic excitation, increasing or decreasing by very small steps the excitation frequency in the spectral neighbourhood of the lowest natural frequencies to characterize non-linear responses in presence of large-amplitude vibrations. The excitation has been provided by an electrodynamical exciter (shaker), model LDS V406 with power amplifier LDS PA100E, connected to the shell by a stinger glued in a position close to the middle of the shell, specifically at $x = 251\,\text{mm}$. A piezoelectric force transducer, model B&K 8200, of mass 21 g, placed on the shaker and connected to the shell by a stinger, measured the force transmitted. The shell response has been measured by using two accelerometers, model B&K 4393, of mass 2.4 g. For all non-linear tests, the two accelerometers have been glued close to the middle of the shell length, specifically at $x = 264\,\text{mm}$, at different angular positions corresponding to an antinode and a node of the excited driven mode to measure the non-linear response. The specific locations of the accelerometers are given in Table 1 for the different modes investigated. The time responses have been measured by using the Difa Scadas II front-end connected to a HP c3000 workstation with the software CADA-X of LMS for signal processing and data analysis; the same front-end has been used to generate the excitation signal. The CADA-X closed-loop control has been used to keep constant the value of the excitation force for any excitation frequency, during the measurement of the non-linear response.

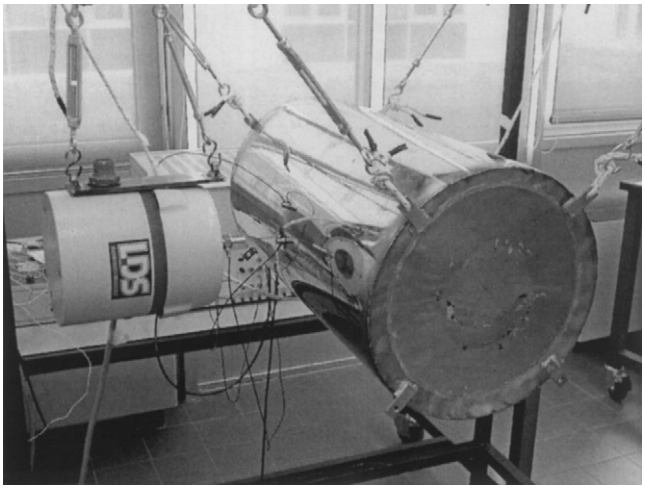

Fig. 1. Photograph of the experimental set-up.

Table 1
Location $R\theta$ of the two accelerometers in large-amplitude vibration tests; excitation at origin $\theta = 0$

Mode	Shell filling	1st accelerometer (mm)	2nd accelerometer (mm)
$n = 5$	Empty	26.5	−21
$n = 6$	Empty	−17.5	22.5
$n = 4$ and 6	Water filled	46.5	−12
$n = 5$	Water filled	30	−17
$n = 7$	Water filled	−7	27
$n = 10$	Water filled	0	24

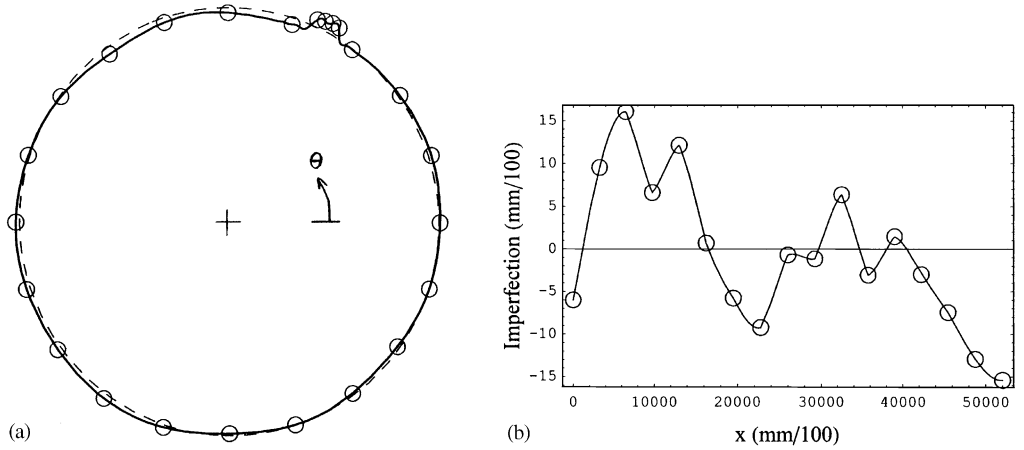

Fig. 2. Geometric imperfections of the shell surface: (a) central circumference (imperfections magnified 10 times); (b) line at $\theta = 60^\circ$. ○, measured point; —, Fourier interpolation; - - -, perfect geometry.

5.1. Geometric imperfections

The shell surface of the tested shell has been measured on a lathe by using a dial gauge on a grid of 100 points, i.e., five equidistant circumferences and 20 positions around each circumference. Moreover, a fine grid of additional 68 points has been measured around the longitudinal weld where small deformations of the shell are present. Fig. 2(a) shows the geometry of the measured central circumference with the magnitude of detected imperfection magnified by a factor 10; in particular, both measured points and their associated Fourier interpolation are given. The origin of the angular co-ordinate θ is taken at the excitation point. The geometric imperfections in the central circumference are mainly localized around the weld at $\theta = 63^\circ$, as shown in Fig. 2(a), with a protuberance of about 0.15 mm. The Fourier series interpolating the measured points of Fig. 2(a) is given in Appendix C. Obviously, Fourier coefficients from measurements on other circumferences are slightly different. Geometric imperfections in the longitudinal direction are plotted in Fig. 2(b) at $\theta = 60^\circ$, i.e., 3° ahead of the longitudinal welding. Results show that deformations are mainly concentrated at the longitudinal weld and at the shell ends, where the annular end plates have been welded to the shell.

6. Modal analysis (linear results)

The frequency response functions (FRFs) have been measured between 100 response points and one single excitation point. Both excitation force and measured responses have been in the radial direction. The response points have been located on a grid of five equidistant circumferences and 20 positions around each circumference; this allows for detection of mode shapes with up to 10 circumferential waves. The experimental modal analysis has been performed by using the software CADA-X 3.5b of LMS and burst-random excitation with the following parameters: burst length, 55% for empty shell, 70% for water-filled shell; frequency resolution 0.15 Hz; 10 averages; uniform windows. The FRFs have been estimated using the H_V technique. The modal parameters have been estimated by using the time domain, least-squares complex exponential technique for the water-filled shell and the frequency domain, direct parameter identification technique for the empty shell. The analysis of the experimental data has been validated by using the modal assurance criterion and the modal phase collinearity.

Due to the axial symmetry of the shell, each asymmetric mode presents two poles in the FRFs associated with orthogonal modes having the same shape but circumferentially rotated by $\pi/(2n)$, i.e., $\cos(n\theta)$ and $\sin(n\theta)$ modes. However, due to the small imperfections of the shell, the two frequencies are not coincident but very close. Many of these couple of modes have been experimentally detected in the low-frequency range.

The sum of the measured FRFs is shown in Fig. 3 with identification of natural modes for both the empty and the water-filled shell. The measured natural frequencies are presented and compared in Figs. 4 and 5 to theoretical calculations with the linear Flügge's theory of shells, e.g., see Ref. [30], both for the empty and water-filled shell. In Figs. 6 and 7 eighth experimental mode shapes with one longitudinal half-wave ($m = 1$) and different number of circumferential waves n are shown for the empty and water-filled shell, respectively. The dashed line represents the 2nd mode, when a couple of modes has been detected. Damping coefficients are given in the figure caption and are sensibly larger for the water-filled shell, except for modes $n = 3$ and 4. However, some inaccuracy in the measurement of damping of these modes, for the empty shell, is accountable for the frequency shift due to the change of position (and therefore added mass) of the accelerometers during the tests. The fundamental mode is ($n = 5$, $m = 1$) for both the empty and the water-filled shell. Theoretical and experimental results are in good agreement both in natural frequencies and mode shapes. This assures that the experimental boundary conditions approximate simple supports with good accuracy. The three-dimensional representation of three measured mode shapes of the water-filled shell is given in Fig. 8.

7. Non-linear results for the empty shell

7.1. Response of perfect shell and effect of imperfections

Numerical calculations have been performed for the fundamental mode ($n = 5$, $m = 1$) of the empty shell tested in the experiments in order to investigate the effect of geometric imperfections of a given shape on the natural frequency and non-linear response.

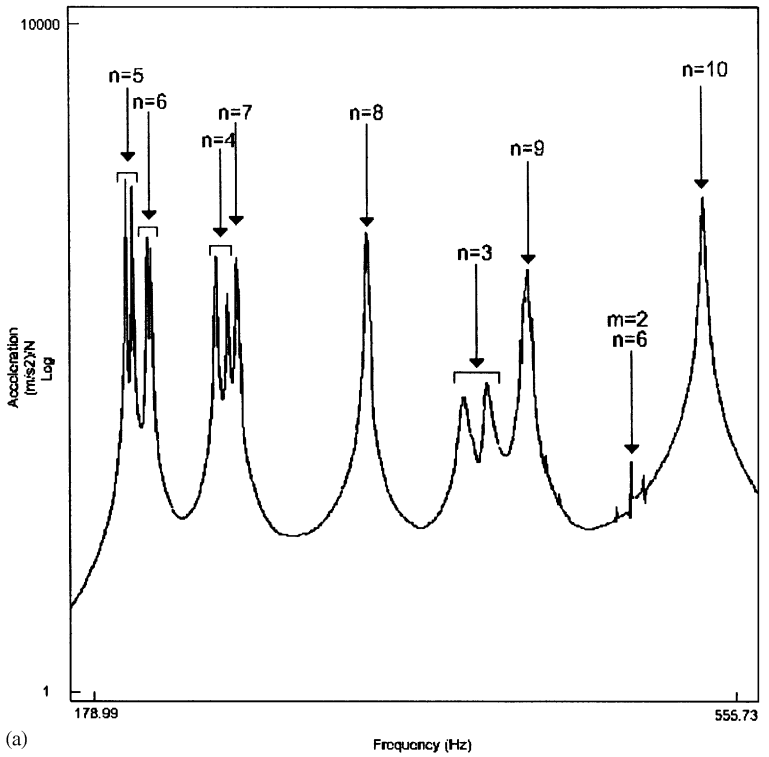

(a)

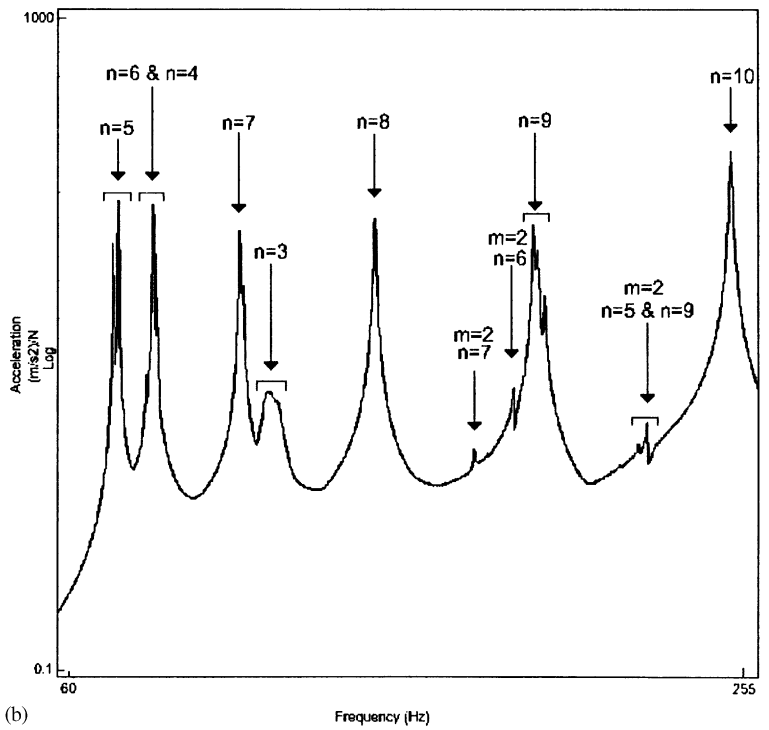

(b)

Fig. 3. Sum of the measured FRFs with identification of natural modes: (a) empty shell; (b) water-filled shell.

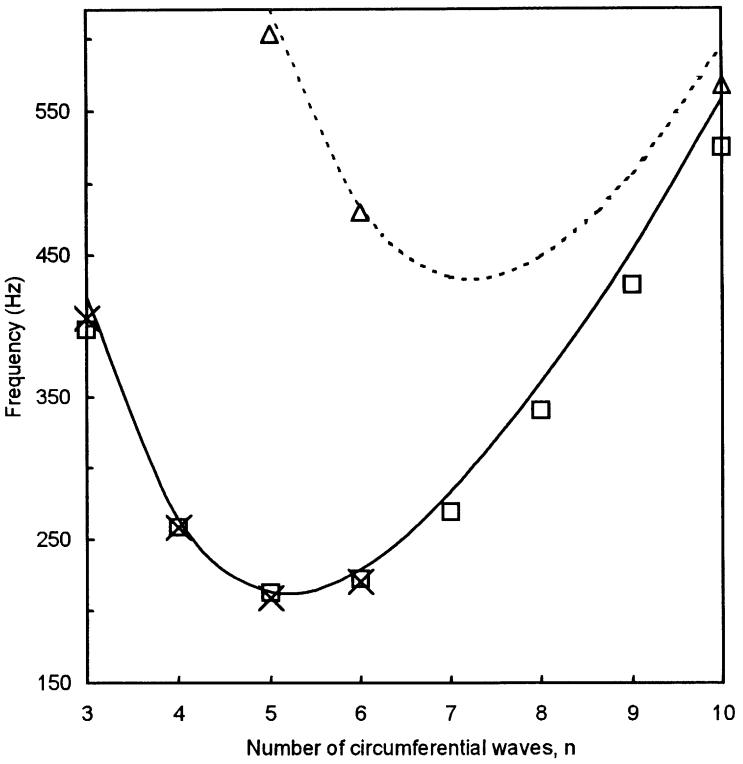

Fig. 4. Theoretical and experimental natural frequencies of the empty shell. Theoretical results: —, $m = 1$; ⋯, $m = 2$. Experimental results: □, $m = 1$; ×, $m = 1$, 2nd mode; △, $m = 2$.

Fig. 9 shows the natural frequency of the fundamental mode of the empty shell versus the amplitude of three different geometric imperfections: (i) axisymmetric imperfection $\tilde{A}_{1,0}$, (ii) asymmetric imperfection $\tilde{A}_{1,n}$ having the same shape of the fundamental mode, and (iii) asymmetric imperfection $\tilde{A}_{1,2n}$ having twice the number of circumferential waves of the fundamental mode. The axisymmetric imperfection does not divide the double eigenvalue associated with the fundamental mode; this is only obtained by asymmetric imperfections. Small positive axisymmetric imperfections (inward Gaussian curvature) decrease the natural frequency, negative axisymmetric imperfections (outward Gaussian curvature) increase it. Moreover, imperfections having twice the number of circumferential waves with respect to the resonant mode have a very large effect on its natural frequency, as indicated in Fig. 9(c); imperfections with the same number of circumferential waves have a smaller effect, but still significant. Imperfections with a number of circumferential waves that is not a multiple of n play a very small role.

The response–frequency relationship of the perfect, empty shell under harmonic point excitation of magnitude 1.5 N is given in Fig. 10 upon assuming modal damping on the fundamental mode $\zeta_{1,n} = 0.0008$. Only the resonant generalized co-ordinates $A_{1,n}(t)$ and $B_{1,n}(t)$ are plotted; the co-ordinate $A_{1,n}(t)$ is the driven mode because it has an antinode at the location of the excitation force; the co-ordinate $B_{1,n}(t)$ is the companion mode. The companion mode has the same shape of the driven mode, but it is angularly rotated by $\pi/(2n)$ and has amplitude different

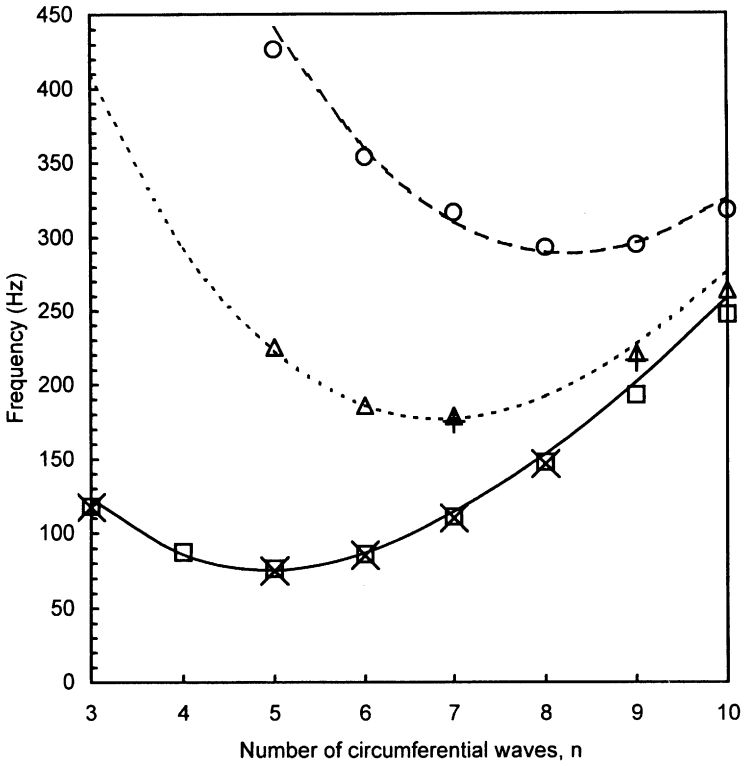

Fig. 5. Theoretical and experimental natural frequencies of the water-filled shell. Theoretical results: —, $m = 1$; ⋯, $m = 2$; - - -, $m = 3$. Experimental results: □, $m = 1$; ×, $m = 1$, 2nd mode; △, $m = 2$; +, $m = 2$, 2nd mode; ○, $m = 3$.

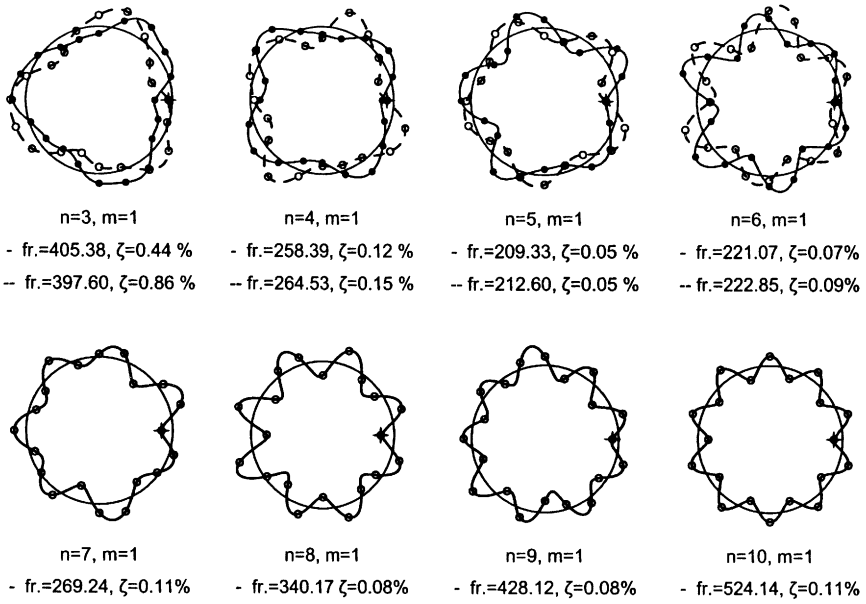

Fig. 6. Experimental modes, empty shell. ○, ● measured points; —, - - - interpolating lines from Fourier analysis; +driving point.

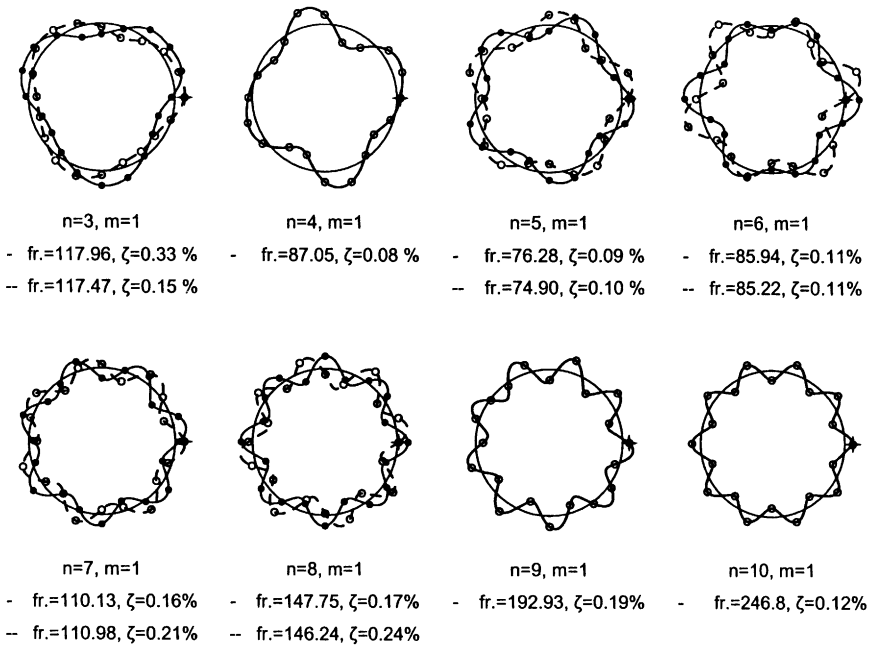

Fig. 7. Experimental modes, water-filled shell. ○, ● measured points; —, - - - interpolating lines from Fourier analysis; + driving point.

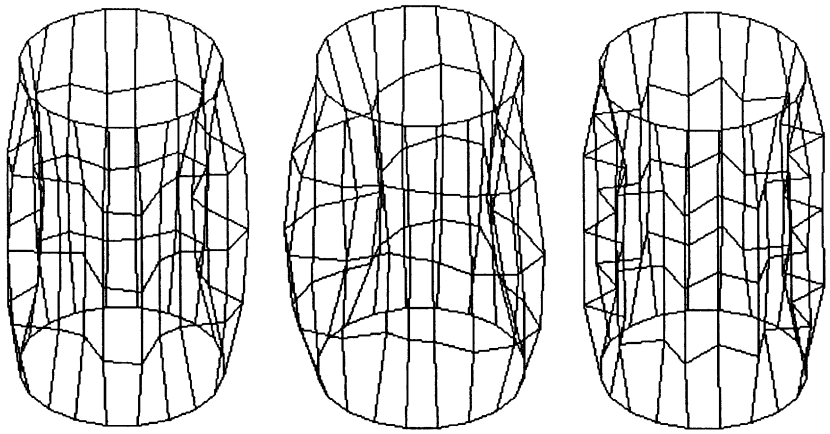

Fig. 8. Three-dimensional representation of measured natural modes with one longitudinal half-wave ($m = 1$) for the water-filled shell; all points at the intersection of two lines have been measured: (a) mode $n = 5$; (b) mode $n = 3$; (c) mode $n = 10$.

from zero only in a small neighbourhood of resonance. It presents a node at the location of the excitation force and therefore it is not directly excited; its amplitude is different from zero only for large-amplitude vibrations, due to non-linear coupling. In the narrow frequency region where

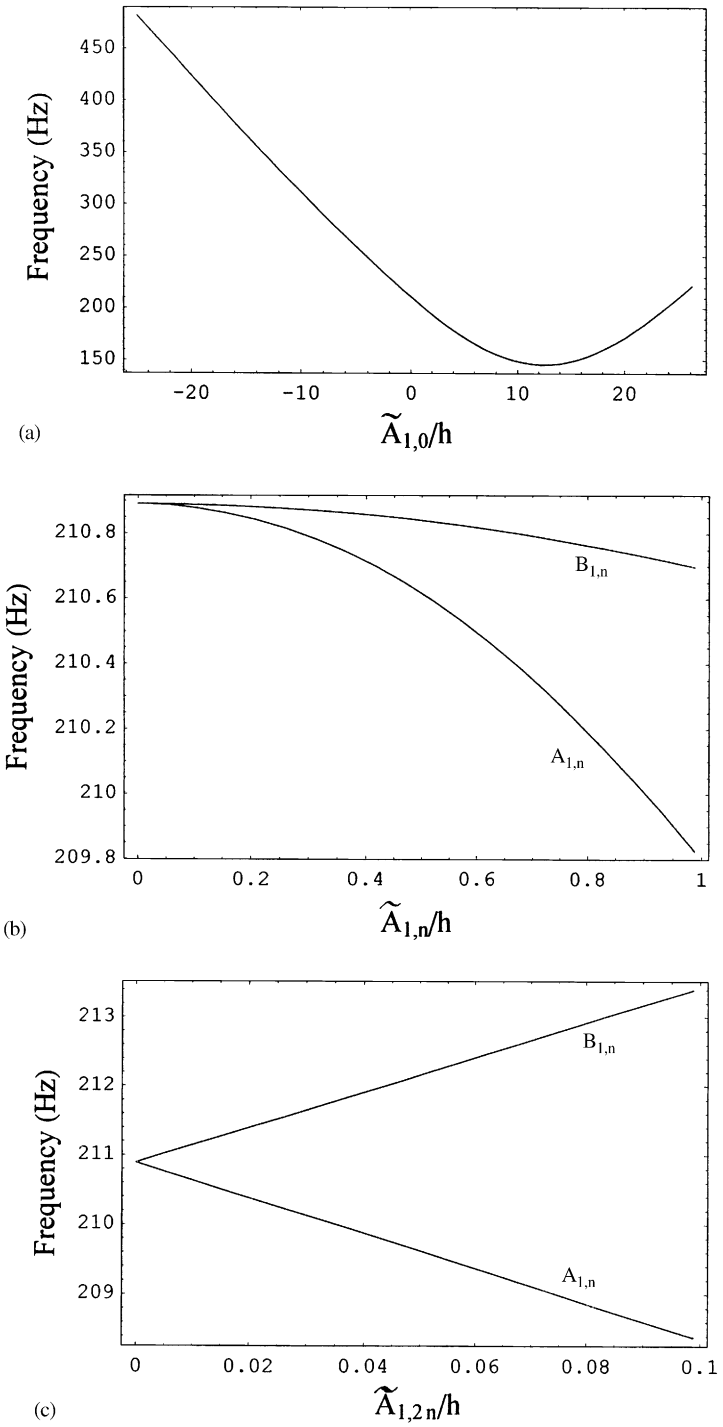

Fig. 9. Natural frequency of the fundamental mode ($n = 5, m = 1$) of the empty shell versus the amplitude of geometric imperfections: (a) axisymmetric imperfection $\tilde{A}_{1,0}$; (b) asymmetric imperfection $\tilde{A}_{1,n}$; (c) asymmetric imperfection $\tilde{A}_{1,2n}$.

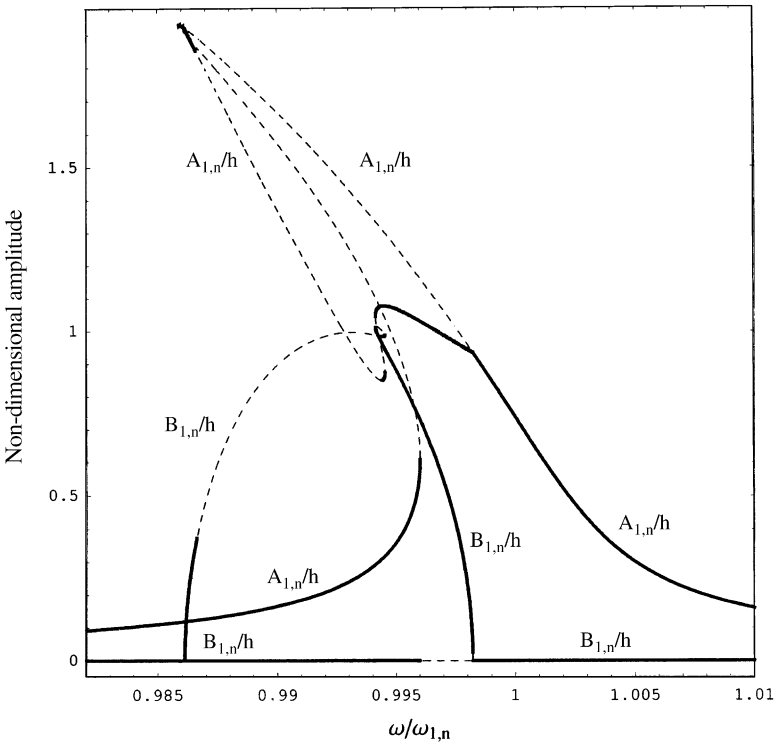

Fig. 10. Response amplitude–frequency relationship of the resonant generalized co-ordinates $A_{1,n}(t)$ and $B_{1,n}(t)$ for the fundamental mode of the perfect, empty shell. The maximum amplitude of $A_{1,n}(t)$, driven mode, and $B_{1,n}(t)$, companion mode, is plotted.

both $A_{1,n}(t)$ and $B_{1,n}(t)$ are different from zero, they give rise to a travelling wave around the shell, as previously discussed in Section 4.1; phase shift between the two co-ordinates is almost $\pi/2$. The response–frequency relationship of the shell in Fig. 10, showing softening type non-linearity, is a well-known result; see e.g., Refs. [4,5,8,10,11,14]. However, the present calculations use a base of 16 modes, practically reaching convergence of the solution.

Asymmetric imperfections with the same shape of the resonant mode have a large effect on the non-linear response. Fig. 11 shows the shell response along with responses of the imperfect shell with $\tilde{A}_{1,n} = 0.5h$ and $\tilde{B}_{1,n} = 0.5h$ (positive or negative asymmetric imperfections give the same result; this is not true for axisymmetric imperfections, see Section 8.1). Results show that the trend of non-linearity is minimally affected in this case, but the travelling wave response is largely modified, due to the fact that natural frequencies of the driven and companion modes do not coincide anymore. Imperfections with $2n$ circumferential waves, where n is the circumferential wavenumber of the mode excited, will be discussed in Section 7.2.

7.2. Comparison of theoretical and experimental results

The fundamental mode of the empty shell has been measured to be divided into a couple of orthogonal modes having the same shape ($n = 5$, $m = 1$) but slightly different frequency, 209.33

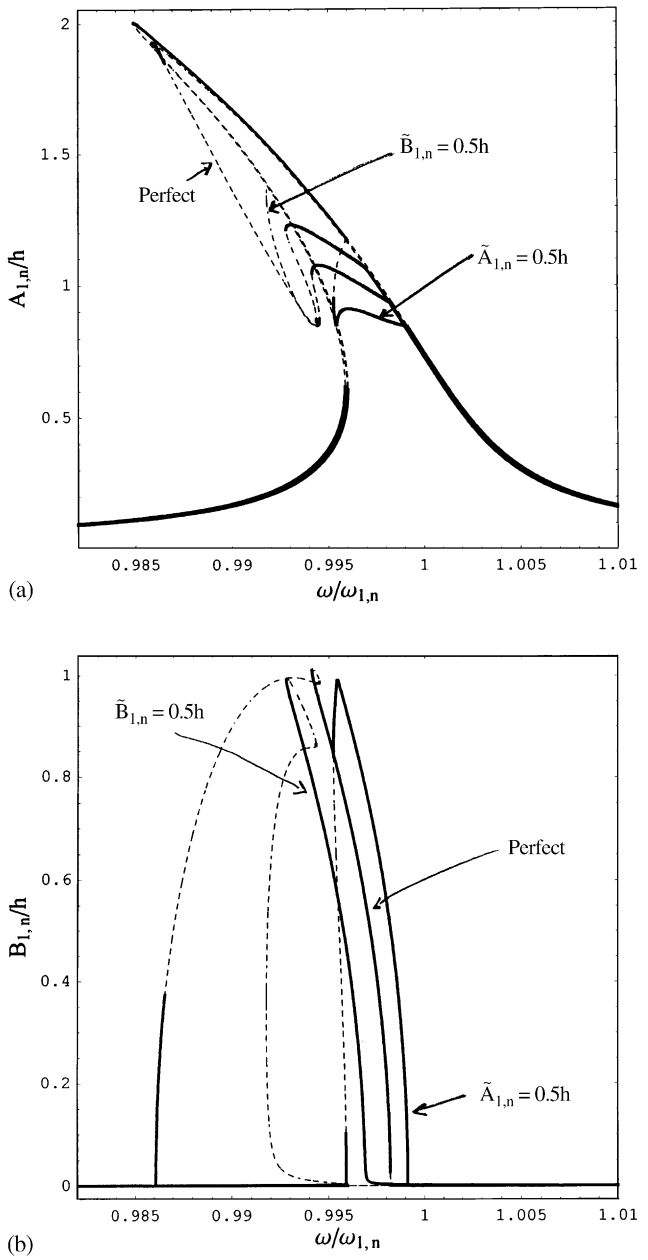

Fig. 11. Response amplitude–frequency relationship of the resonant generalized co-ordinates for the fundamental mode of the empty shell; perfect shell and shell with geometric imperfections $\tilde{A}_{1,n}$ and $\tilde{B}_{1,n}$: (a) driven mode $A_{1,n}(t)$; (b) companion mode $B_{1,n}(t)$.

and 212.6 Hz. The small difference in the frequency of the two, virtually identical, modes is attributed to imperfections of the test specimen, reported in Section 5.1, and to the mass of the sensors glued to the wall of the shell. In addition, imperfections affect the position of the mode

shapes on the circumference with respect to the excitation point, making it more difficult to find nodes. Without imperfections, the first one of the couple of modes presents an antinode at the excitation point; the second mode presents there a node. The node closest to the excitation point has been experimentally determined for each of these two modes and an accelerometer has been

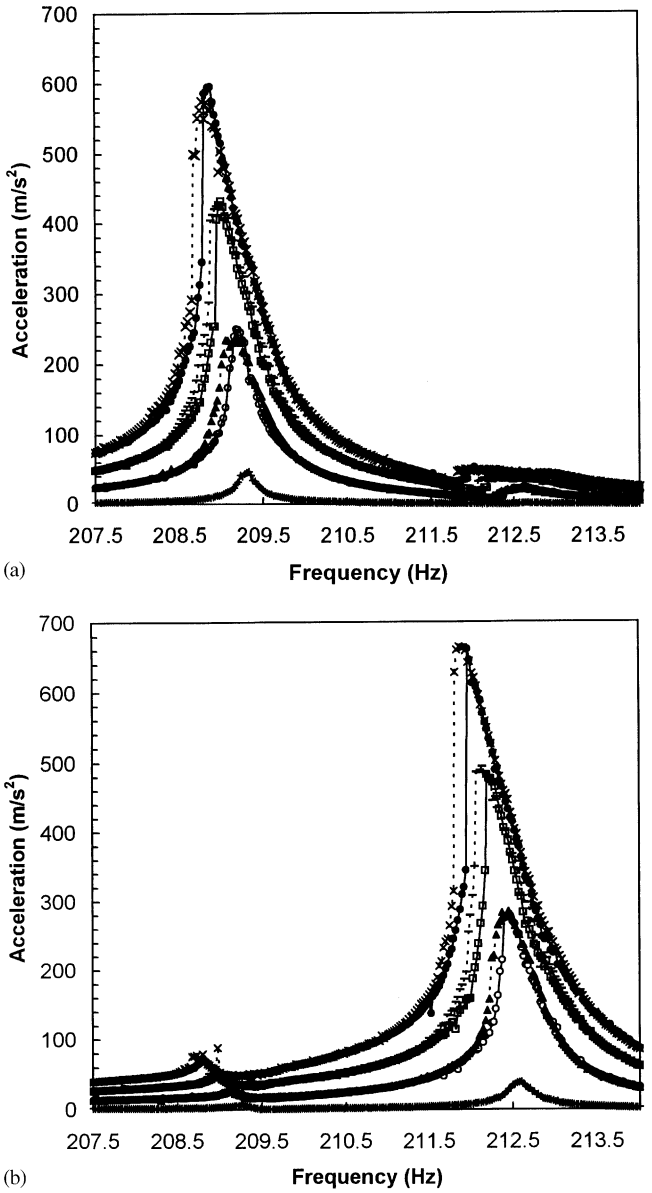

Fig. 12. Experimentally measured acceleration versus excitation frequency for the fundamental mode of the empty shell: (a) 1st accelerometer; (b) 2nd accelerometer. —+—, force 0.025 N; —○—, force 0.25 N up (i.e., increasing the excitation frequency); --▲--, force 0.25 N down (i.e., decreasing the excitation frequency); —□—, force 0.5 N up; --▪--, force 0.5 N down; —●—, force 0.75 N up; --×--, force 0.75 N down.

placed there. Therefore each one of the two accelerometers is at a node of one mode, corresponding to an antinode of the other, orthogonal mode. The location of the accelerometers is given in Table 1. It can be immediately observed that both accelerometers are considerably far from the excitation point. Therefore both modes are directly driven by the excitation. The projections of the excitation force on $A_{1,n}(t)$ and $B_{1,n}(t)$ give $0.64\tilde{f}$ and $0.768\tilde{f}$, respectively.

Figs. 12(a) and (b) show the accelerations measured by the two accelerometers around the fundamental frequency versus the excitation frequency for four different force levels: 0.025, 0.25, 0.5, and 0.75 N. The closed-loop control used in the experiments keeps the excitation force constant after filtering the signal from the load cell in order to use only the harmonic component with the given excitation frequency. The measured accelerations reported in Fig. 12 have been filtered in order to eliminate any frequency except the excitation frequency. Experiments have been performed both increasing and decreasing the excitation frequency; the frequency resolution used in this case is 0.025 Hz. The hysteresis between the two curves (up = increasing frequency; down = decreasing frequency) is clearly visible. Sudden increments (jumps) of the vibration amplitude are observed upon increasing and decreasing the excitation frequency; these are characteristic of a weak softening-type non-linearity. When the vibration amplitude is equal to 0.7 times the shell thickness, the peak of the response appears for a frequency lower of about 0.37% with respect to the linear one (i.e., the one measured with force 0.025 N). The travelling wave response around the shell, associated with significant acceleration measured by both accelerometers at the same frequency, is not observed in this case because the separation of the two modes with the same shape is too large for the maximum force level reached in the experiments.

The phase relationships between the two accelerations (measured positive outwards) and the force input (measured positive inwards) are given in Fig. 13.

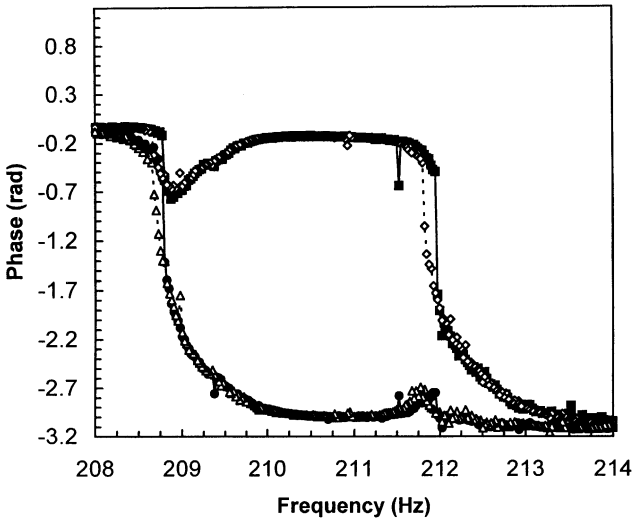

Fig. 13. Experimentally measured response phase–frequency curves for the fundamental mode of the empty shell; force 0.75 N. —●—, 1st accelerometer up; —■—, 2nd accelerometer up; – –△– –, 1st accelerometer down; – –◇– –, 2nd accelerometer down.

The measured accelerations have been converted to displacements, dividing by the excitation circular frequency squared, and have been plotted in Fig. 14 together with the theoretical responses for the case with a force level of 0.75 N; normalization of frequency with respect to $\omega_{1,n} = 212.6 \times 2\pi$ has been performed. When comparing filtered experimental results to theoretical results only co-ordinates $A_{1,n}(t)$ and $B_{1,n}(t)$ must be considered because the others, which have higher frequency as observed in Section 2, are eliminated by the filter. The theoretical curves have been computed by including the geometric imperfection $\tilde{A}_{1,2n} = 0.072h$, which is the value needed to reproduce the frequency difference between the two modes ($n = 5$, $m = 1$); this value is not too far from the geometric imperfection with 10 circumferential waves measured on the central circumference, which is $0.11h$, as reported in Appendix C. The modal damping used to calculate the theoretical curves is $\zeta_{1,n} = 0.00077$ (0.077%) for $A_{1,n}$ and $\zeta_{1,n} = 0.00084$ (0.084%) for $B_{1,n}$ and these have been identified by matching the maximum value of the measured response. The agreement between the theoretical curves and the experimental results is particularly good.

The second mode shape of the empty shell is ($n = 6$, $m = 1$). Also in this case the natural frequencies are split to 221.07 and 222.85 Hz. The locations of the two accelerometers (i.e., of nodes of the two modes) are given in Table 1. The measured accelerations have been converted to displacements and have been plotted in Fig. 15 together with the theoretical responses for the case with a force level of 1.25 N; normalization of frequency with respect to $\omega_{1,n} = 222.85 \times 2\pi$ has been performed. The geometric imperfection $\tilde{A}_{1,2n} = 0.053h$ has been used to reproduce the frequency difference between the two modes. The modal damping used to calculate the theoretical curves is $\zeta_{1,n} = 0.00143$ for $A_{1,n}$ and $\zeta_{1,n} = 0.00095$ for $B_{1,n}$ and these have been identified similarly as for the fundamental mode. The agreement between the theoretical curves and the experimental results is also good in this case. In contrast to the fundamental mode, a small travelling wave response has been observed close to the two resonances. However, the vibration amplitude of the two generalized co-ordinates is far from being the same for any frequency in the range investigated. Therefore the travelling wave response is much smaller than the standing wave response.

8. Non-linear results for the water-filled shell

8.1. Response of perfect shell and effect of imperfections

Calculations have been performed for the fundamental mode ($n = 5$, $m = 1$) of the water-filled shell tested in the experiments. Fig. 16 shows the natural frequency of the fundamental mode of the water-filled shell versus the amplitude of five different geometric imperfections: (i) axisymmetric imperfection $\tilde{A}_{1,0}$, (ii) ovalization imperfection $\tilde{A}_{1,2}$, (iii) asymmetric imperfection $\tilde{A}_{1,n}$ having the same shape of the fundamental mode, (iv) asymmetric imperfection $\tilde{A}_{1,2n}$ having twice the number of circumferential waves of the fundamental mode, and (v) asymmetric imperfections with 16 circumferential waves, which is not a multiple of n. Results show that ovalization imperfections and asymmetric imperfections with 16 circumferential waves have a very small effect on the natural frequency of the fundamental mode; moreover, they do not split the double eigenvalue. Similar to the case of an empty shell, the imperfection giving the larger effect on natural frequency is $\tilde{A}_{1,2n}$. Axisymmetric imperfection does not split the double eigenvalue

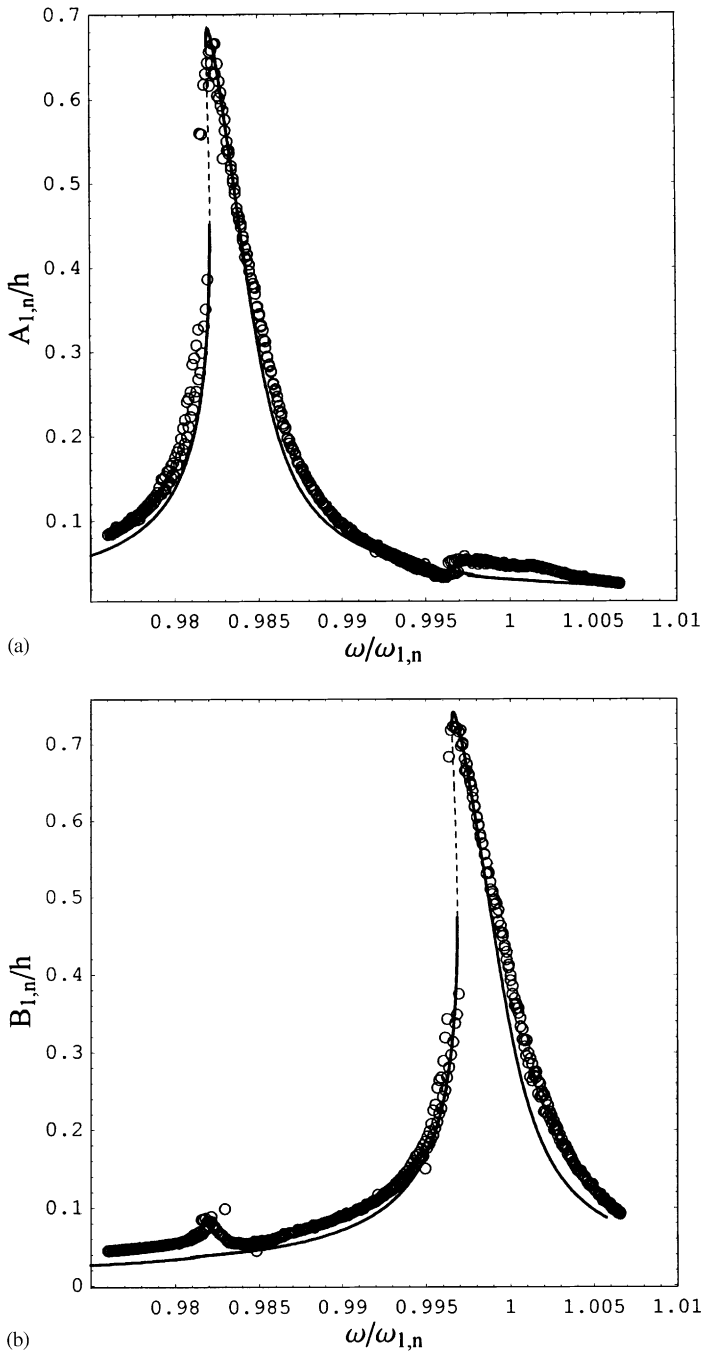

Fig. 14. Response amplitude–frequency relationship for the fundamental mode of the empty shell; force 0.75 N. ○, experimental data; ——, stable theoretical solutions; – – –, unstable theoretical solutions: (a) displacement/h from the 1st accelerometer; (b) displacement/h from the 2nd accelerometer.

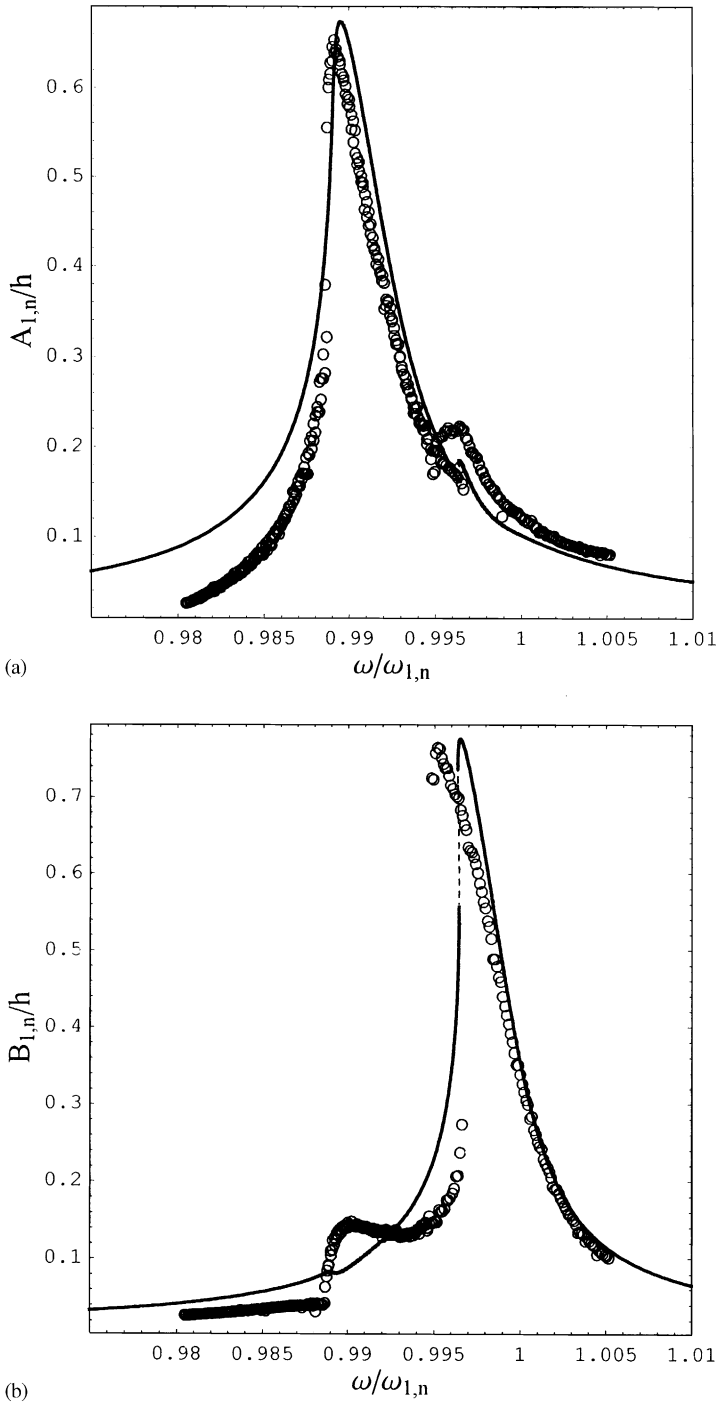

Fig. 15. Response amplitude–frequency relationship for the mode ($n = 6$, $m = 1$) of the empty shell; force 1.25 N. ○, experimental data; ——, stable theoretical solutions; – – –, unstable theoretical solutions: (a) displacement/h from the 1st accelerometer; (b) displacement/h from the 2nd accelerometer.

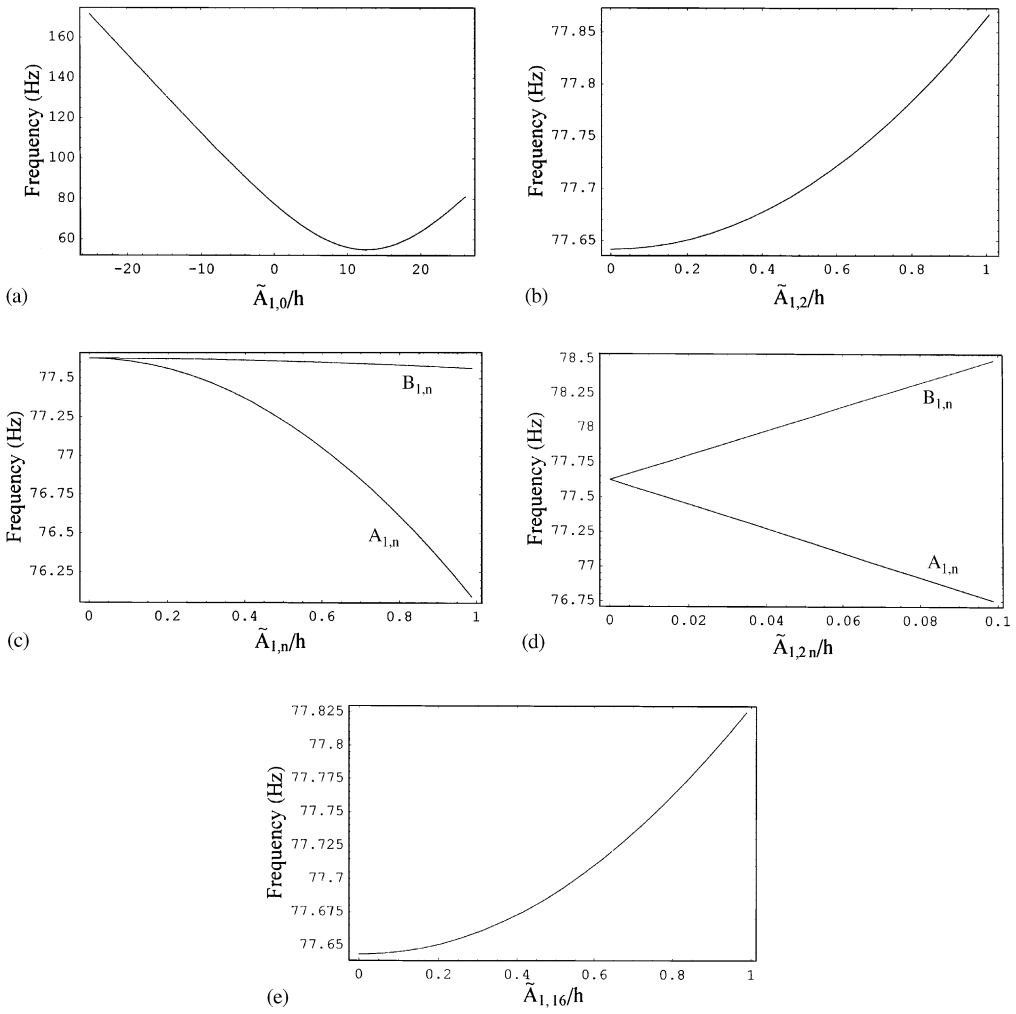

Fig. 16. Natural frequency of the fundamental mode ($n = 5$, $m = 1$) of the water-filled shell versus the amplitude of geometric imperfections: (a) Axisymmetric imperfection $\tilde{A}_{1,0}$; (b) ovalization imperfection $\tilde{A}_{1,2}$; (c) asymmetric imperfection $\tilde{A}_{1,n}$; (d) asymmetric imperfection $\tilde{A}_{1,2n}$; (e) asymmetric imperfection $\tilde{A}_{1,16}$.

associated with the fundamental mode; small positive imperfections (inward Gaussian curvature) decrease the natural frequency, negative (outward Gaussian curvature) imperfections increase it.

The response–frequency relationship of the fundamental mode of the perfect, water-filled shell under harmonic point excitation of magnitude 3 N is given in Fig. 17 upon assuming modal damping $\zeta_{1,n} = 0.0017$. The response–frequency relationship of the shell in Fig. 17 shows a largely increased softening behaviour, due to the contained water, with respect to the one of the fundamental mode of the same, empty shell given in Fig. 10. Fig. 17 presents a main branch "1" corresponding to zero amplitude of the companion mode $B_{1,n}(t)$; this branch has pitchfork bifurcations at $\omega/\omega_{1,n} = 0.9714$ and 1.0018 where branch "2" appears. This new branch

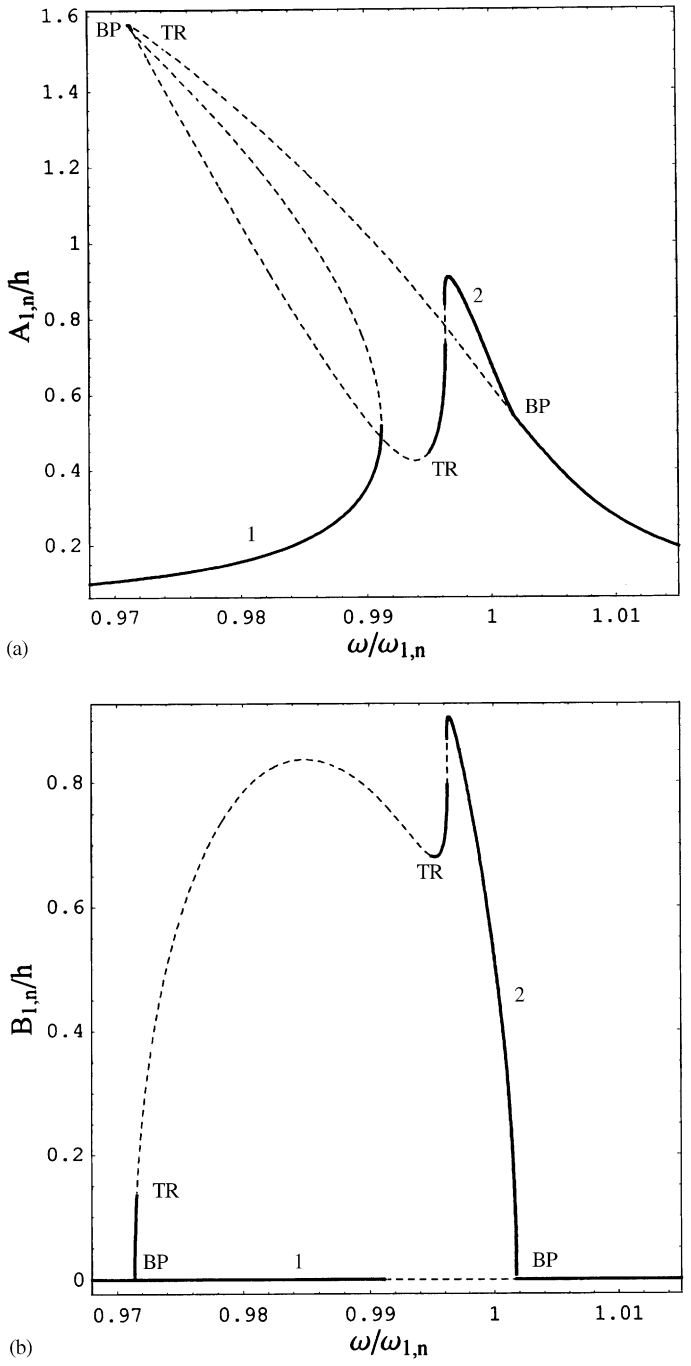

Fig. 17. Response amplitude–frequency relationship of the resonant generalized co-ordinates $A_{1,n}(t)$ and $B_{1,n}(t)$ for the fundamental mode of the perfect, water-filled shell: (a) maximum amplitude of $A_{1,n}(t)$, driven mode; (b) maximum amplitude of $B_{1,n}(t)$, companion mode. 1, branch "1"; 2, branch "2"; BP, pitchfork bifurcation; TR, Neimark–Sacker bifurcations.

corresponds to participation of both $A_{1,n}(t)$ and $B_{1,n}(t)$ that gives travelling wave response. Branch "2" loses stability through two Neimark–Sacker (torus) bifurcations at $\omega/\omega_{1,n} = 0.9716$ and 0.9949. No stable response is indicated in Fig. 17 for $0.9911 < \omega/\omega_{1,n} < 0.9949$; in fact, only simple-periodic responses are indicated as stable solutions in Fig. 17. The response of the shell for $0.9911 < \omega/\omega_{1,n} < 0.9949$ is modulated in amplitude (quasiperiodic).

The effect of axisymmetric imperfection with magnitude equal to the shell thickness on the non-linear response is limited, as shown in Fig. 18. Fig. 19 shows that ovalizaton of an amplitude twice as big as the shell thickness is even less important. However, asymmetric imperfections with the same shape of the resonant mode have a large effect on the non-linear response, as shown in Figs. 20 and 21. Similar to what observed in Fig. 11 for the empty shell, the trend of non-linearity is minimally affected in this case, but the travelling wave response is completely modified. It is easy to conclude that imperfections having the same shape of the mode excited and with the same

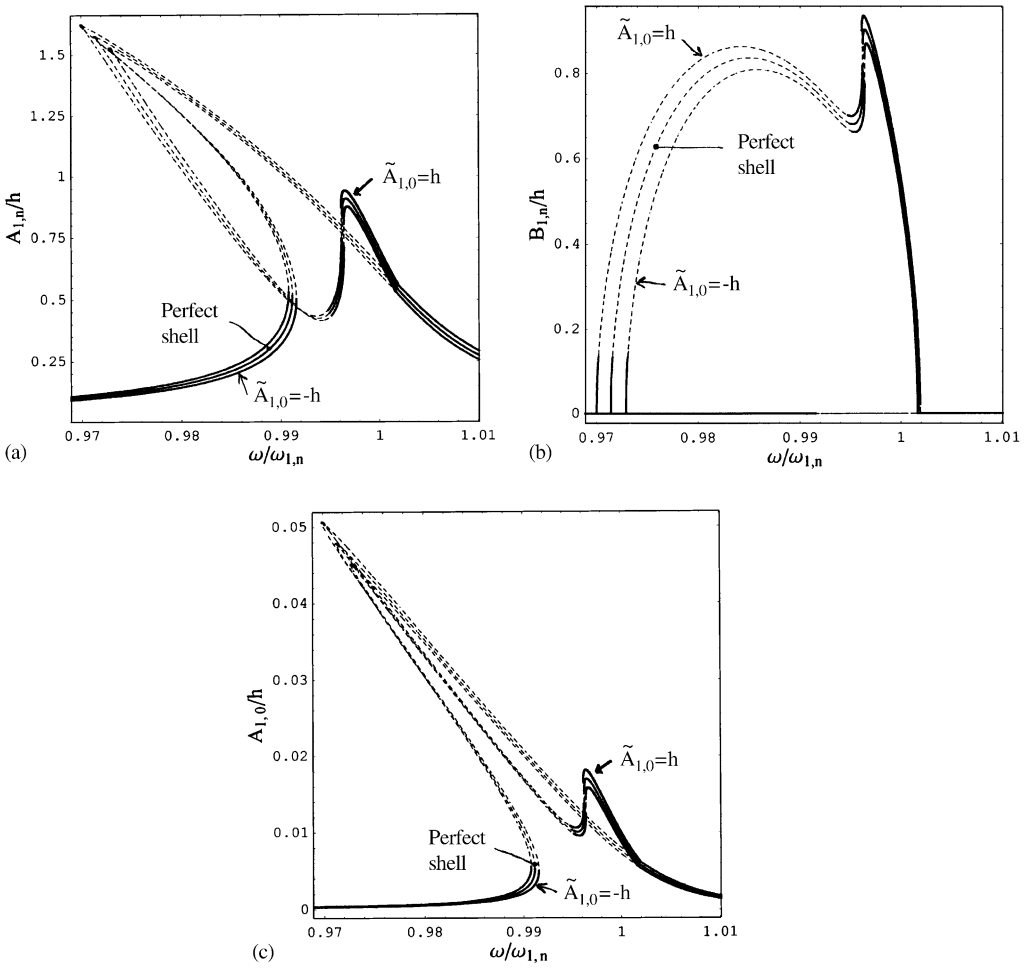

Fig. 18. Response amplitude–frequency relationship of the main generalized co-ordinates for the fundamental mode of the water-filled shell; perfect shell and shell with axisymmetric geometric imperfections $\tilde{A}_{1,0} = \pm h$: (a) driven mode $A_{1,n}(t)$; (b) companion mode $B_{1,n}(t)$; (c) first axisymmetric mode $A_{1,0}(t)$.

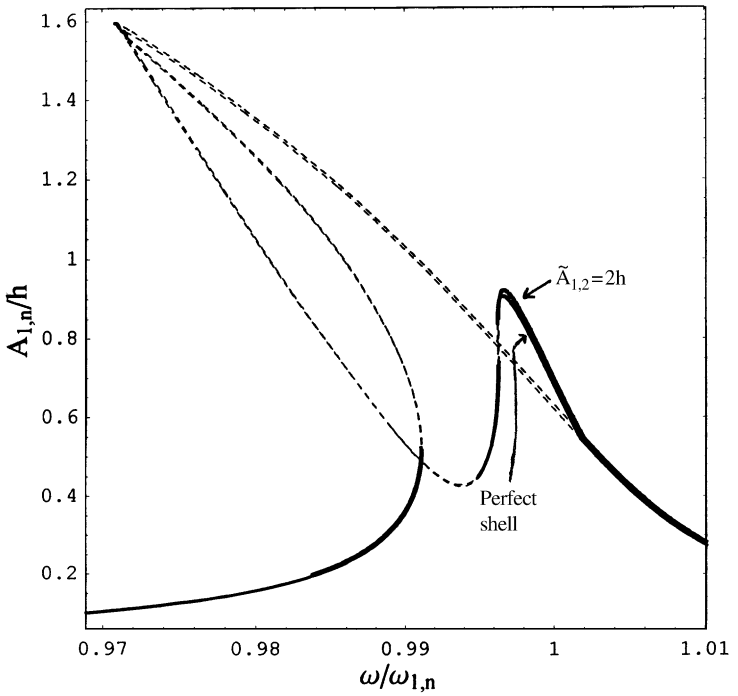

Fig. 19. Response amplitude–frequency relationship of the driven mode $A_{1,n}(t)$ for the fundamental mode of the water-filled shell; perfect shell and shell with ovalization $\tilde{A}_{1,2} = 2h$.

order of magnitude of the shell thickness (the magnitude $0.5h$ has been simulated here) are able to change almost completely the shell response around a resonance. Imperfections with $2n$ circumferential waves, where n is the circumferential wavenumber of the mode excited, will be discussed in Section 8.2.

8.2. Comparison of theoretical and experimental results in the frequency domain

The fundamental mode ($n = 5, m = 1$) of the water-filled shell has been measured to be split in a couple of orthogonal modes having the same shape but slightly different frequency, 74.9 and 76.28 Hz, whereas the theoretical value is 76.16 Hz, according to Flügge's theory of shells and 77.64 Hz according to Donnell's shallow-shell theory. Of these two modes, the one with the lowest frequency will be referred as the 1st mode; the other will be the 2nd mode. The location of the shapes of these two modes with respect to the excitation point has been experimentally determined and an accelerometer has been placed at a node of each mode, corresponding to an antinode of the 2nd mode. The locations of the two accelerometers are given in Table 1; as a consequence, the projections of the excitation force on $A_{1,n}(t)$ and $B_{1,n}(t)$ give $0.543\tilde{f}$ and $0.84\tilde{f}$, respectively. Therefore, both modes are directly excited.

Fig. 22 shows the accelerations measured by the two accelerometers versus the excitation frequency for five different force levels: 0.1, 1.5, 3, 4.5 and 6 N. The measured accelerations reported in Fig. 22 have been filtered in order to eliminate any other frequency, except the

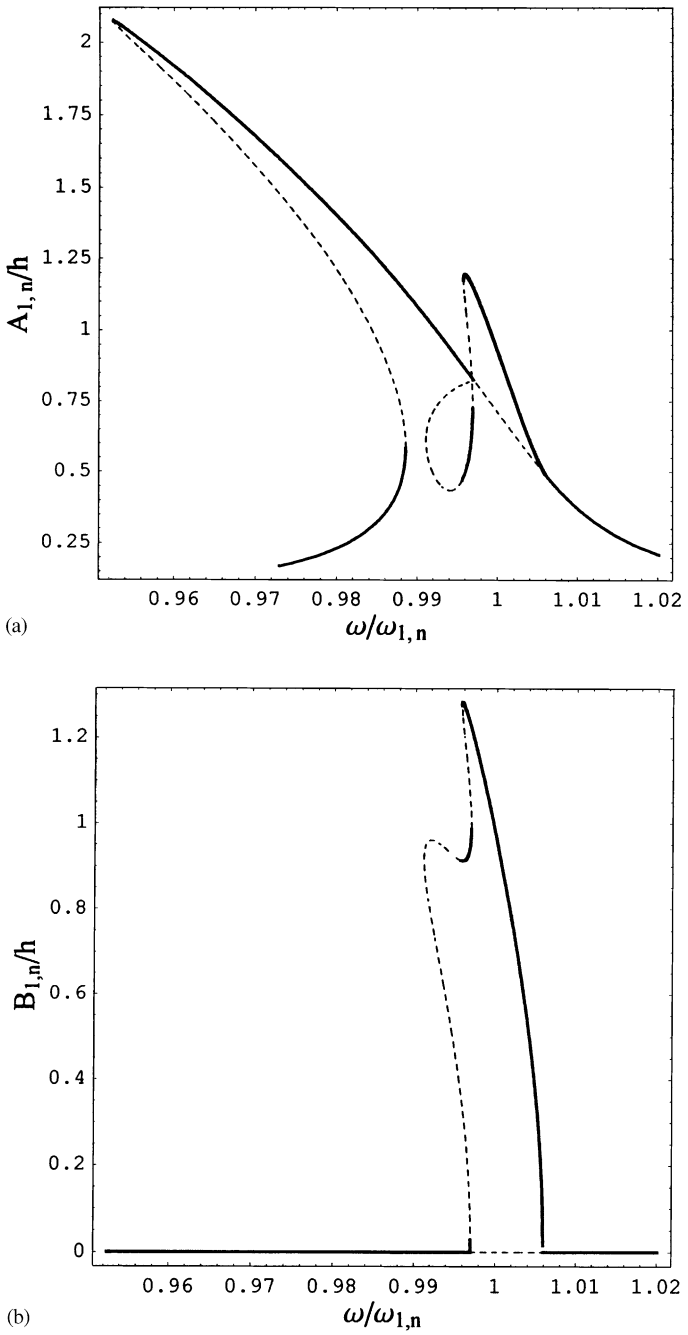

Fig. 20. Response amplitude–frequency relationship of the resonant generalized co-ordinates for the fundamental mode of the water-filled shell; shell with geometric imperfection $\tilde{A}_{1,n} = 0.5h$: (a) driven mode $A_{1,n}(t)$; (b) companion mode $B_{1,n}(t)$.

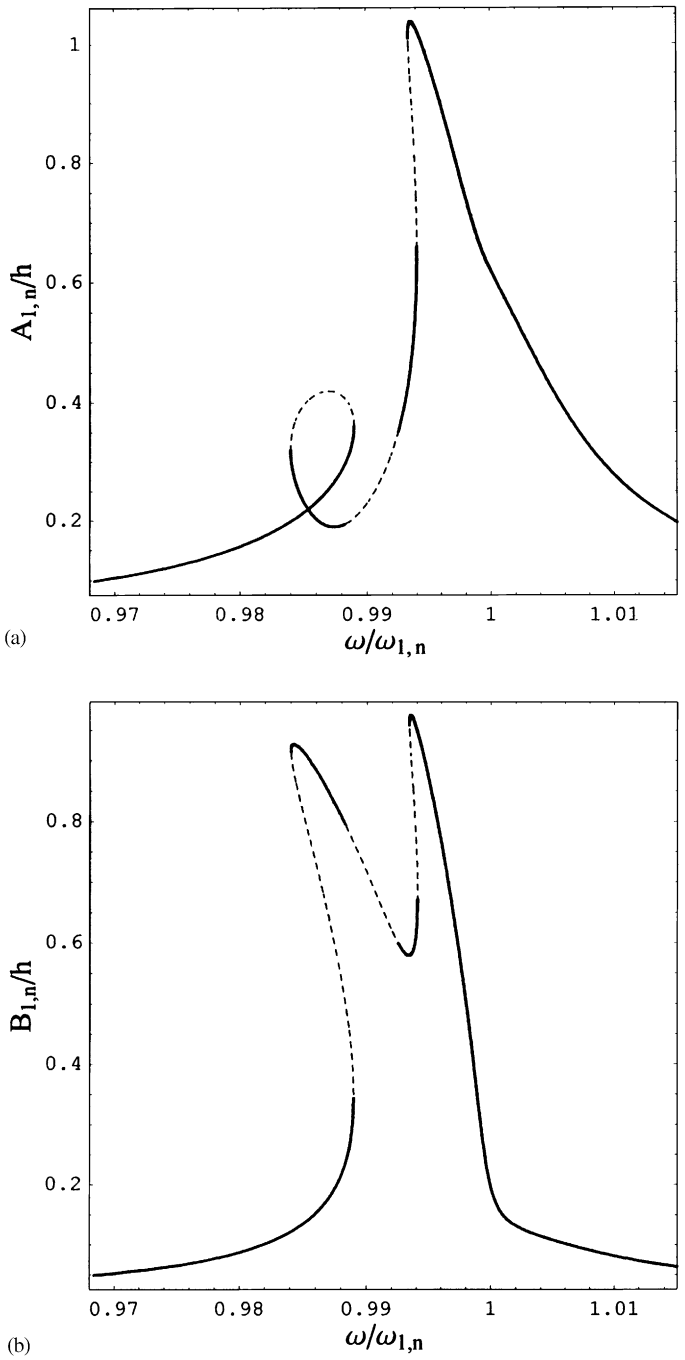

Fig. 21. Response amplitude–frequency relationship of the resonant generalized co-ordinates for the fundamental mode of the water-filled shell; shell with geometric imperfection $\tilde{B}_{1,n} = 0.5h$: (a) driven mode $A_{1,n}(t)$; (b) companion mode $B_{1,n}(t)$.

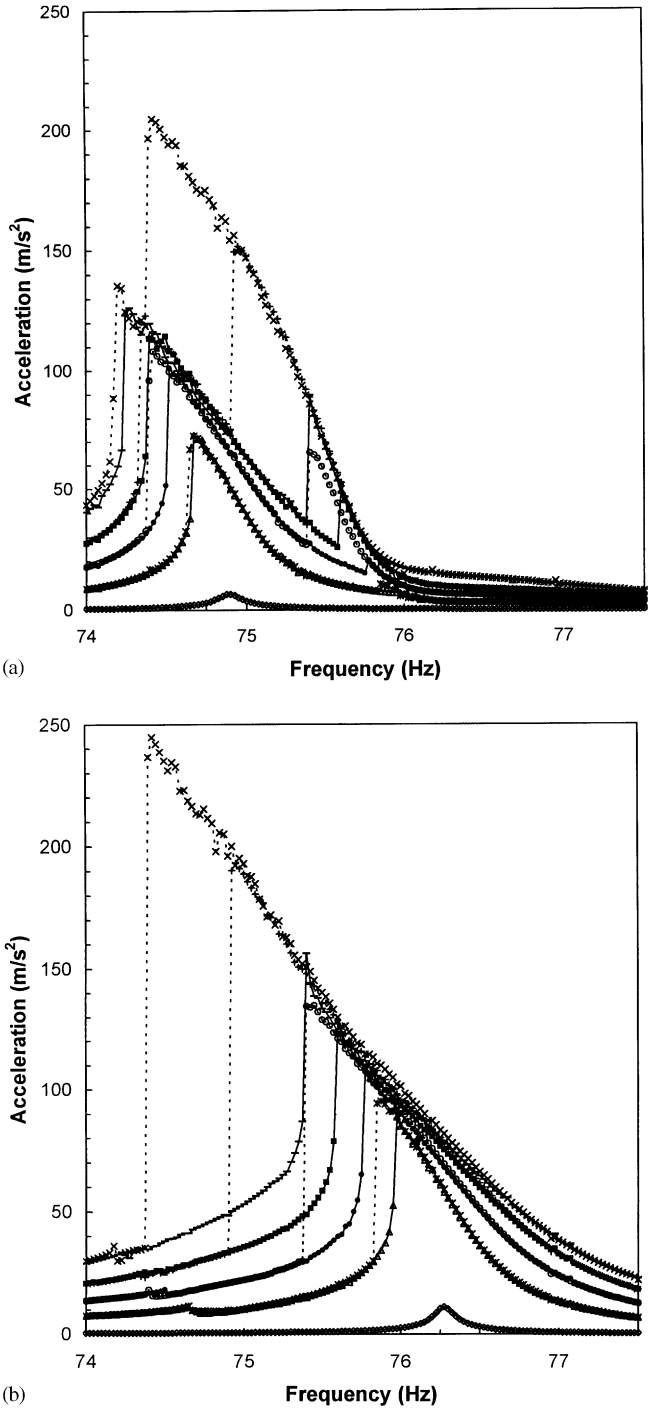

Fig. 22. Experimentally measured acceleration versus excitation frequency for the fundamental mode of the water-filled shell: (a) 1st accelerometer; (b) 2nd accelerometer. —◇—, force 0.1 N; —△—, force 1.5 N up (i.e., increasing the excitation frequency); – –∗– –, force 1.5 N down (i.e., decreasing the excitation frequency); —●—, force 3 N up; – –○– –, force 3 N down; —■—, force 4.5 N up; – –+– –, force 4.5 N down; – –▪– –, force 6 N up; – –×– –, force 6 N down.

excitation frequency. Experiments have been performed both increasing and decreasing the excitation frequency and hysteresis is clearly visible. The frequency resolution used in this case is 0.025 Hz. Sudden increments (jumps) of the vibration amplitude are observed upon changing the excitation frequency; these are characteristic of softening type non-linearity, which is much stronger than in the corresponding case for the empty shell (see Fig. 12). When the vibration amplitude is equal to the shell thickness, the peak of the response appears for a frequency lower of more than 1% with respect to the linear one (i.e., the one measured with force 0.1 N). The travelling wave response around the shell has been detected in a relatively large-frequency range around the resonance, especially for the excitation force of 6 N.

The phase relationships between the two accelerations (measured positive outwards) and the force input (measured positive inwards) are given in Fig. 23; the phase shift between the first and second accelerometer is about $\pi/2$ when travelling wave response arises.

The measured accelerations have been converted to displacements, dividing by the excitation circular frequency squared, and have been plotted in Figs. 24–26 together with the theoretical responses for the case with force levels of 0.1 (linear case), 3 and 6 N, respectively; normalization of frequency with respect to $\omega_{1,n} = 76.28 \times 2\pi$ has been performed. The co-ordinate $A_{1,n}$ has resonance for the first mode; $B_{1,n}$ has resonance for the second mode. The theoretical curves have been computed by including the geometric imperfection $\tilde{A}_{1,2n} = 0.0817h$, which is the value needed to reproduce the frequency difference between the two modes ($n = 5$, $m = 1$); this value is close enough to the geometric imperfection with 10 circumferential waves measured on the central circumference, which is $0.11h$ (see Appendix C). The modal damping used to calculate the theoretical curves is $\zeta_{1,n} = 0.001$ and 0.00091 for $A_{1,n}$ and $B_{1,n}$, respectively, for a force of 0.1 N; $\zeta_{1,n} = 0.0017$ (0.17%) for both $A_{1,n}$ and $B_{1,n}$ for a force of 3 N; and $\zeta_{1,n} = 0.0029$ and 0.00058 for $A_{1,n}$ and $B_{1,n}$, respectively, for a force of 6 N. These values have been identified by matching the maximum value of the measured response. The agreement between the theoretical curves and the experimental results is good for all the force magnitudes analyzed (force 1.5 and 4.5 N are not

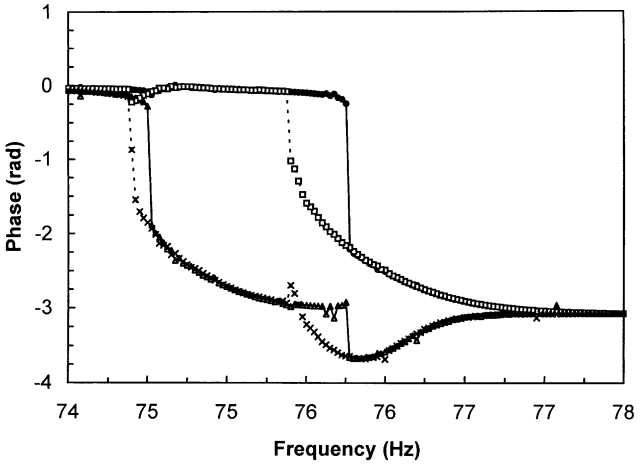

Fig. 23. Experimentally measured response phase–frequency curves for the fundamental mode of the water-filled shell; force 3 N. —▲—, 1st accelerometer up; —●—, 2nd accelerometer up; – – × – –, 1st accelerometer down; – –□– –, 2nd accelerometer down.

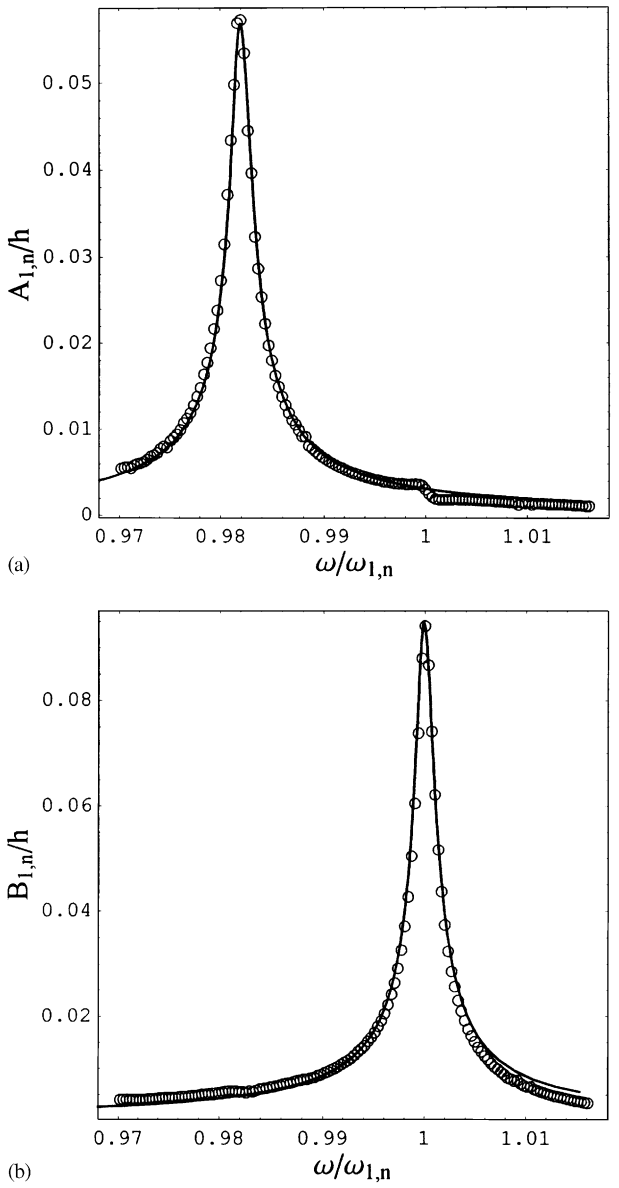

Fig. 24. Response amplitude–frequency relationship for the fundamental mode of the water-filled shell; force 0.1 N, which gives linear behaviour. ○, experimental data; ——, stable theoretical solutions: (a) displacement/h from the 1st accelerometer; (b) displacement/h from the 2nd accelerometer.

reported here for sake of brevity) for both first and second modes (it is excellent for the 2nd mode) and for both co-ordinates $A_{1,n}$ and $B_{1,n}$. Only the co-ordinate $A_{1,n}$ participates in the 1st resonance ($B_{1,n} \cong 0$); on the other hand, both co-ordinates $A_{1,n}$ and $B_{1,n}$ participate in the 2nd resonance and travelling wave response arises ($A_{1,n}$ has almost the same value of $B_{1,n}$ for force of 6 N). In fact, the

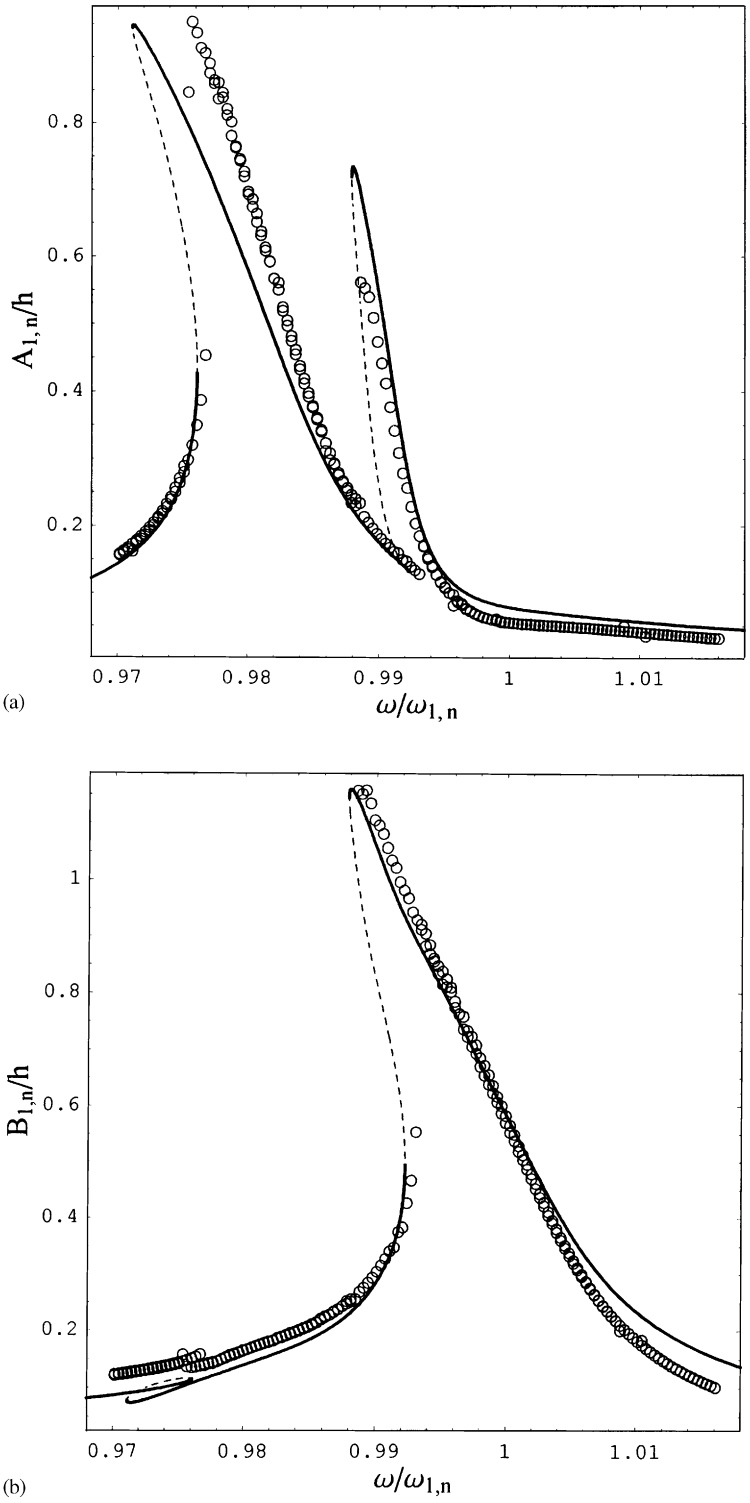

Fig. 25. Response amplitude–frequency relationship for the fundamental mode of the water-filled shell; force 3 N. ○, experimental data; ——, stable theoretical solutions; – – –, unstable theoretical solutions: (a) displacement/h from the 1st accelerometer; (b) displacement/h from the 2nd accelerometer.

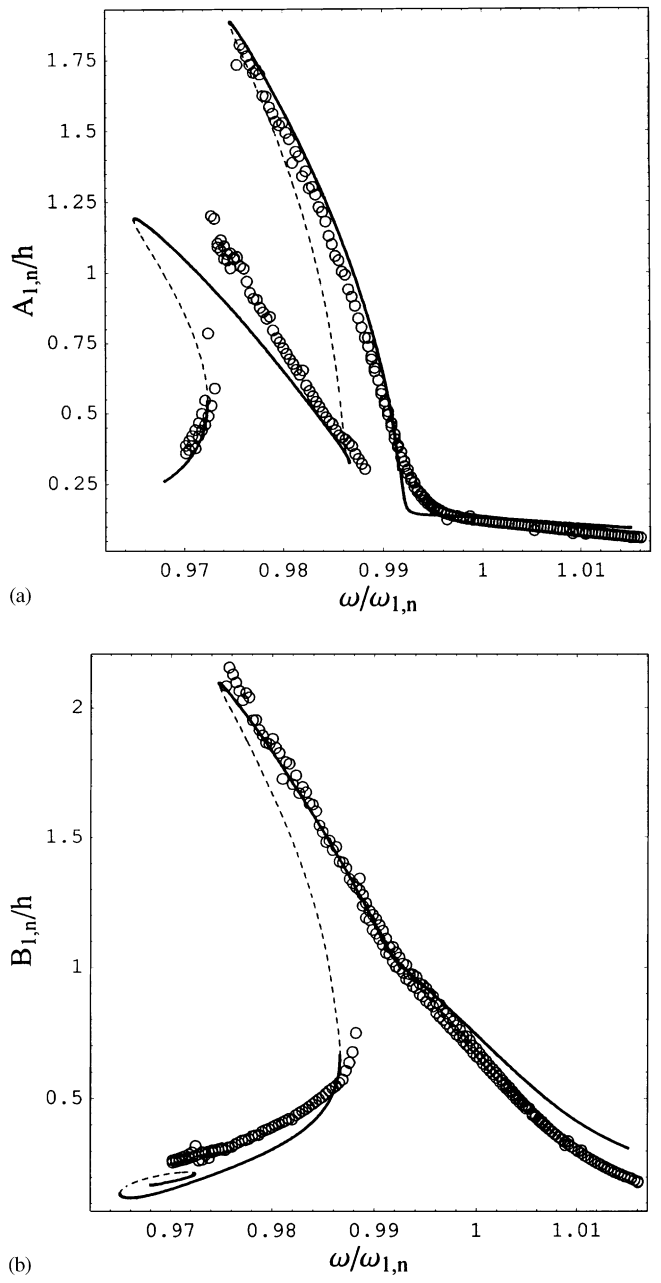

Fig. 26. Response amplitude–frequency relationship for the fundamental mode of the water-filled shell; force 6 N. ○, experimental data; ——, stable theoretical solutions; – – –, unstable theoretical solutions: (a) displacement/h from the 1st accelerometer; (b) displacement/h from the 2nd accelerometer.

softening behaviour of the water-filled shell helps interaction between the two modes for the 2nd resonance. In fact, due to the softening behaviour, the resonance of co-ordinate $B_{1,n}$ moves to smaller frequency, coming very close to the resonance of $A_{1,n}$.

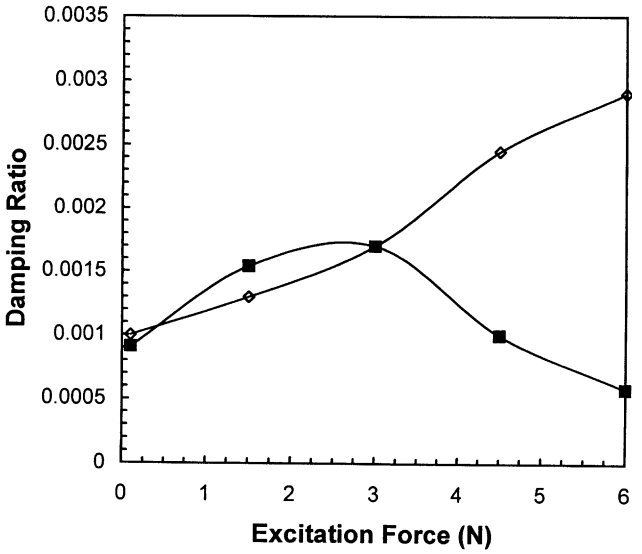

Fig. 27. Damping ratio of the fundamental mode of the water-filled shell versus the excitation force. —◇—, co-ordinate $A_{1,n}(t)$; —■—, co-ordinate $B_{1,n}(t)$.

Fig. 27 shows the change in the identified modal damping versus the excitation force, which is related to the vibration amplitude. The damping of the co-ordinate $A_{1,n}$ increases almost linearly with the force magnitude; this seems due to the fact that no travelling wave response is observed for the resonance of $A_{1,n}$. Damping coefficients of co-ordinates $A_{1,n}$ and $B_{1,n}$ have similar values for forces of 0.1 and 1.5 N, and have exactly the same value for the force of 3 N. For this force magnitude the travelling wave response becomes significant (the amplitude of $A_{1,n}$ becomes about 1/2 of $B_{1,n}$ around resonance of the second mode) and damping on the co-ordinate $B_{1,n}$ largely decreases for larger forces.

The modes of the water-filled shell immediately following in frequency the fundamental mode are ($n = 4$, $m = 1$) and ($n = 6$, $m = 1$), respectively. These two modes have very close natural frequencies and therefore must be studied together because of their complex interaction. The natural frequencies of mode ($n = 4$, $m = 1$) are split to 84.20 and 87.05 Hz; those of mode ($n = 6$, $m = 1$) are 85.22 and 85.94 Hz. The locations of the two accelerometers used in the experiments are given in Table 1. In particular, accelerometers have been placed close to nodes (or antinodes) of mode ($n = 4$, $m = 1$). Mode ($n = 6$, $m = 1$) has an antinode close to the excitation point, as it should be for a perfect shell. The measured linear behaviour of the system is given in Fig. 28 for a force excitation of 0.1 N; it shows that four modes are present in a frequency range of 3 Hz. A satisfactorily comparison between numerical and experimental results for a force of 5 N is given in Fig. 29. No difference is observed in this case between measured acceleration obtained by increasing and decreasing the excitation frequency. The main difference with the previous case is that almost no softening-type non-linearity is observed. This is due to the non-linear interaction between modes with different number of circumferential waves ($n = 4$ and 6) having almost coincident natural frequency. The mode expansion used in the calculations employed modes with four and six circumferential modes. Numerical results have been computed with modal damping

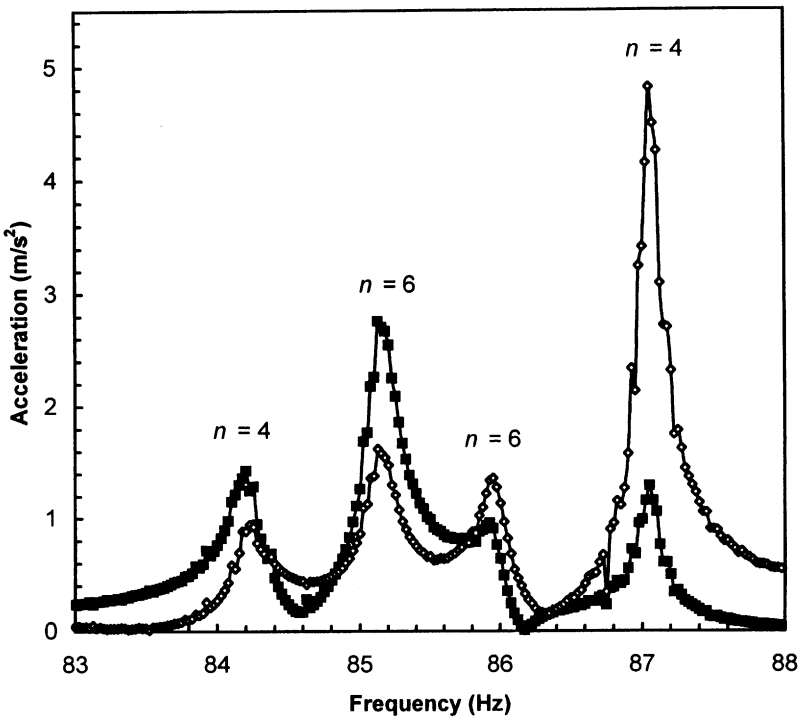

Fig. 28. Experimentally measured acceleration versus excitation frequency for modes ($n = 4$ and 6, $m = 1$) of the water-filled shell; force 0.1 N, which gives linear behaviour. —■—, 1st accelerometer; —◇—, 2nd accelerometer.

$\zeta_{1,4} = 0.0035$ for both $A_{1,4}$ and$B_{1,4}$, and with $\zeta_{1,6} = 0.0023$ for both $A_{1,6}$ and $B_{1,6}$. Frequencies have been normalized with respect to 87.05 Hz. A simplification in the numerical study of this case was the introduction of a small perturbation to the linear part of the equations in order to reproduce the split in the natural frequencies for modes $n = 4$ and 6 instead of using geometric imperfections.

The next mode in frequency is ($n = 7$, $m = 1$). Natural frequencies are split to 110.125 and 110.975 Hz. Locations of the two accelerometers are given in Table 1, as in the previous cases. It can be observed that the first accelerometer is close to the excitation point; therefore the co-ordinate $A_{1,n}$, reproducing the first accelerometer, is mainly driven and $B_{1,n}$, second accelerometer, receives a much smaller force, about $\frac{1}{3}$. Comparison between numerical and experimental results for a force of 1.5 N is given in Fig. 30. The softening behaviour is clearly shown, even if it is weak in this case, due to the relatively small vibration amplitude reached. Companion mode participation is quite large for the small vibration amplitude reached and gives rise to travelling wave response. The main difference between the travelling wave response observed for the fundamental mode and the one found in this case is that now the companion mode has a larger (but very close) frequency with respect to the driven mode. Numerical results have been computed with modal damping $\zeta_{1,n} = 0.003$ for $A_{1,n}$ and $\zeta_{1,n} = 0.002$ for $B_{1,n}$; geometric imperfection $\tilde{A}_{1,2n} = 0.1h$ has been used to reproduce the split frequencies; this value is in strong agreement with the measured imperfection $0.103h$ reported in Appendix C.

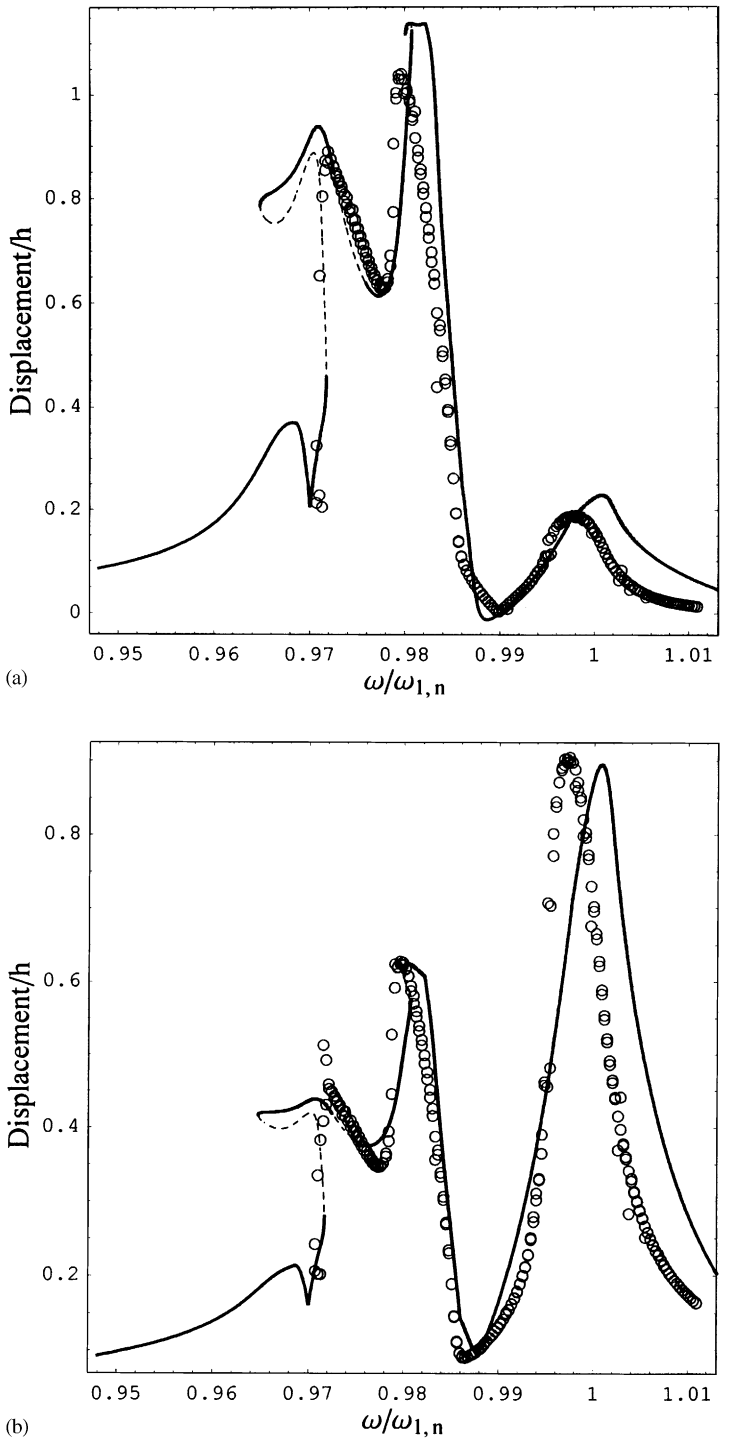

Fig. 29. Response amplitude–frequency relationship for modes ($n = 4$ and 6, $m = 1$) of the water-filled shell; force 5 N. ○, experimental data; ——, stable theoretical solutions; – – –, unstable theoretical solutions: (a) displacement/h from the 1st accelerometer; (b) displacement/h from the 2nd accelerometer.

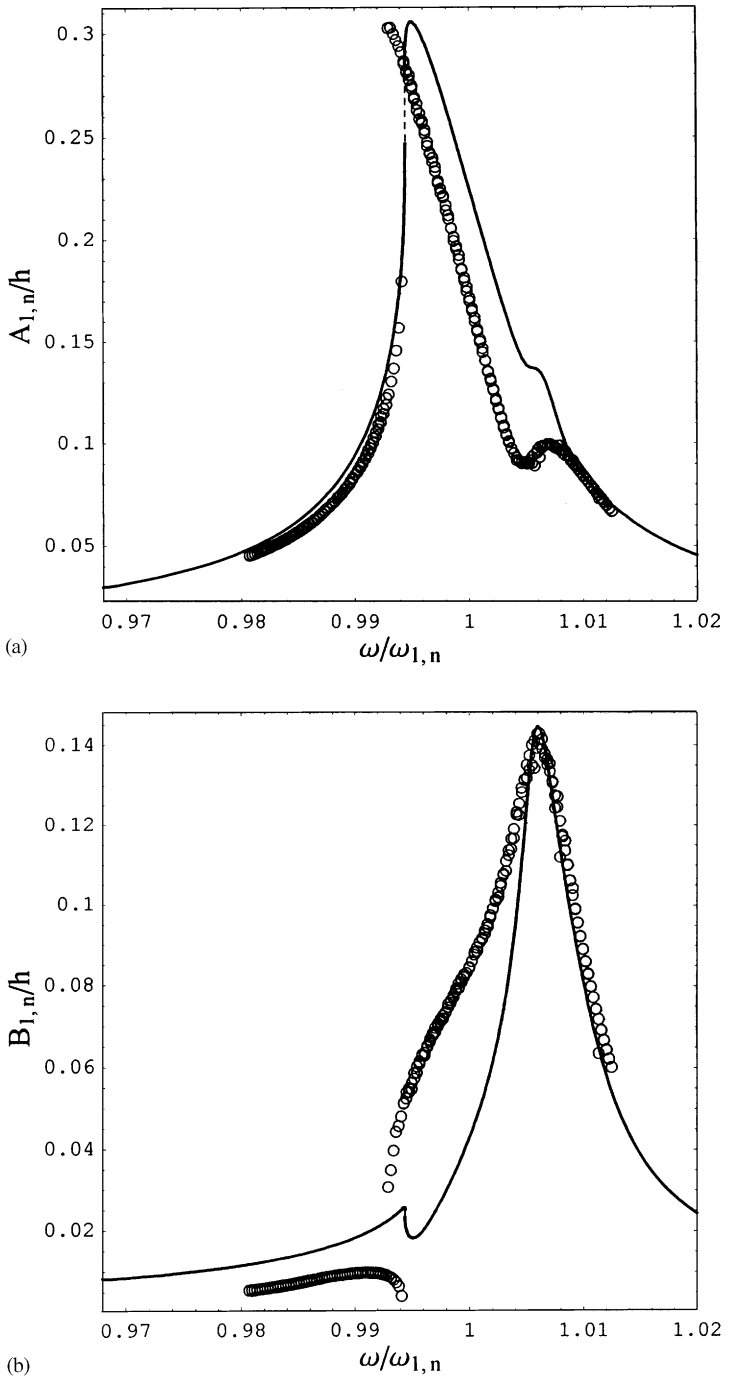

Fig. 30. Response amplitude–frequency relationship for mode ($n = 7$, $m = 1$) of the water-filled shell; force 1.5 N. ○, experimental data; ——, stable theoretical solutions; – – –, unstable theoretical solutions: (a) displacement/h from the 1st accelerometer; (b) displacement/h from the 2nd accelerometer.

The last mode investigated is ($n = 10$, $m = 1$). This case is interesting because the measured frequency separation between the couple of modes is very small. Moreover, the positions of nodes and antinodes where the two accelerometers have been placed (see Table 1) show that $A_{1,n}(t)$ is directly excited (driven mode) and $B_{1,n}(t)$ is only minimally excited (companion mode). Therefore, instead of using small geometric imperfections to reproduce perfectly the experimental results, calculations have been performed for a perfect shell. The measured accelerations have been converted to displacements, dividing by the excitation circular frequency squared, and have been plotted in Fig. 31 together with the theoretical responses for the case with force level 1.5 N; normalization of frequency with respect to $\omega_{1,n} = 246.8 \times 2\pi$ has been performed. The modal damping used to calculate the theoretical curves is $\zeta_{1,n} = 0.0023$ for $A_{1,n}$ and $\zeta_{1,n} = 0.0025$ for $B_{1,n}$. The agreement between the theoretical and experimental results is strong. Around the resonance the amplitudes of $A_{1,n}(t)$ and $B_{1,n}(t)$are close, with $B_{1,n}(t)$ smaller than $A_{1,n}(t)$; in this frequency range the shell response is a travelling wave around the circumference.

The measured response of the shell for force of 3 N is shown in Fig. 32. It is particularly interesting to note that amplitudes of $A_{1,n}(t)$ and $B_{1,n}(t)$ are coincident in this case in a frequency range of almost 2 Hz around the resonance. The companion mode participation grows with the vibration amplitude (and the magnitude of the excitation) from zero to the driven mode curve; after this point, driven and companion mode amplitudes increase simultaneously, giving rise to a pure travelling wave response. The measured accelerations, converted to displacements, have been plotted in Fig. 33 together with the theoretical responses for the case with a force level of 3 N. The modal damping used to calculate the theoretical curves is $\zeta_{1,n} = 0.003$ for both $A_{1,n}$ and $B_{1,n}$. The agreement between the theoretical and experimental results is good. The main branch "1" corresponds to zero vibration amplitude of the companion mode $B_{1,n}(t)$; this branch has pitchfork bifurcations at $\omega/\omega_{1,n} = 0.9791$ and 1.0043 where branch "2" appears. Branch "2" loses stability through two Neimark-Sacker (torus) bifurcations at $\omega/\omega_{1,n} = 0.9795$ and 0.9944. No stable response is indicated in Fig. 33 for $0.9871 < \omega/\omega_{1,n} < 0.9944$; in fact only simple-periodic responses are indicated as stable solutions in Fig. 33. The calculated response of the shell for $0.9871 < \omega/\omega_{1,n} < 0.9944$ is modulated in amplitude (quasiperiodic); small modulations have been measured during experiments; however, they become apparent with increasing the force excitation; amplitude modulated response will be discussed in Section 8.3.

8.3. Comparison of theoretical and experimental results in the time domain

The time response of mode ($n = 10$, $m = 1$) for force excitation of 14 N and excitation frequency 240.5 Hz is shown in Fig. 34 representing amplitude modulations. The frequency of modulations is very small, about 2.1 Hz. Presence of amplitude-modulated vibrations is predicted by the model for mode ($n = 10$, $m = 1$). Negative (inward) accelerations are larger than positive (outward) accelerations of about 13%; this phenomenon is due to significant axisymmetric oscillation of the shell, which takes place inwards with twice the excitation frequency. In fact, axisymmetric modes have been used in the mode expansion of the solution because they are non-linearly coupled to asymmetric modes. From the mechanical point of view, in order to have large-amplitude oscillations of the shell without stretching significantly the shell circumference (the shell is very stiff to in-plane loads), dynamic contraction of the mean circumference is necessary; this phenomenon generates the double-frequency inward axisymmetric oscillation of the shell.

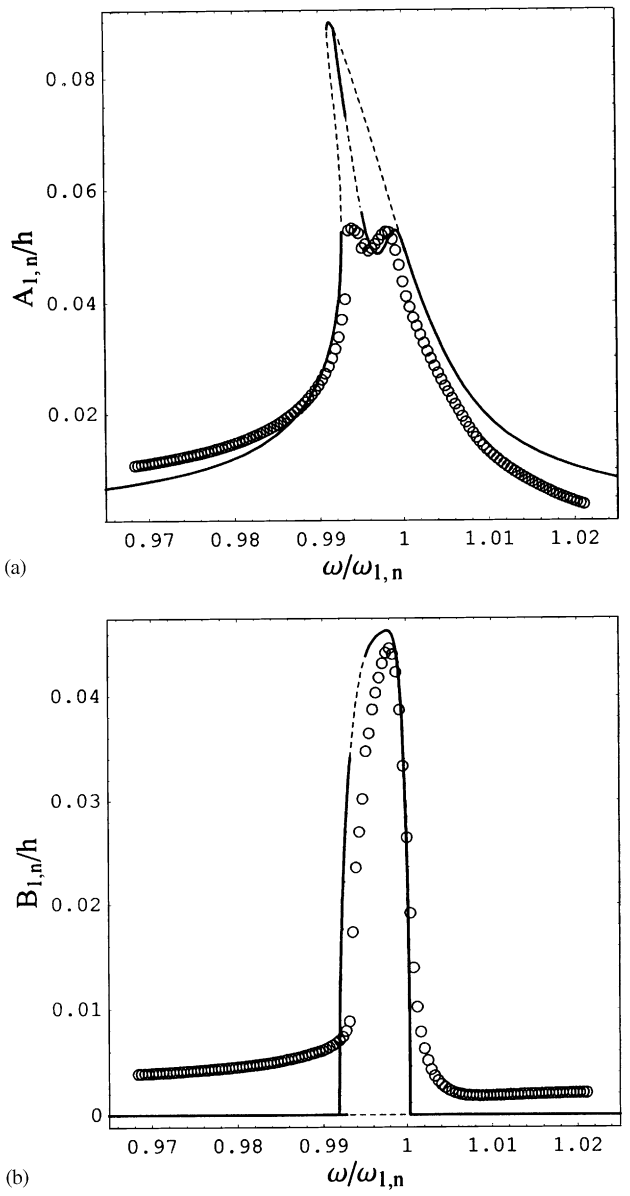

Fig. 31. Response amplitude–frequency relationship for mode ($n = 10$, $m = 1$) of the water-filled shell; force 1.5 N. ○, experimental data; ——, stable theoretical solutions; – – –, unstable theoretical solutions: (a) displacement/h from the 1st accelerometer; (b) displacement/h from the 2nd accelerometer.

The experimental force input and accelerations for the fundamental mode ($n = 5$, $m = 1$) of the water-filled shell are shown in Fig. 35 versus time for excitation of magnitude 3 N and frequency 75.375 Hz measured by decreasing the excitation frequency (down). In these conditions, the shell response is the one obtained immediately after the big jump (sudden decrement of the response amplitude) on the left of peak in Fig. 22(b) for a force of 3 N. The input force simulates accurately

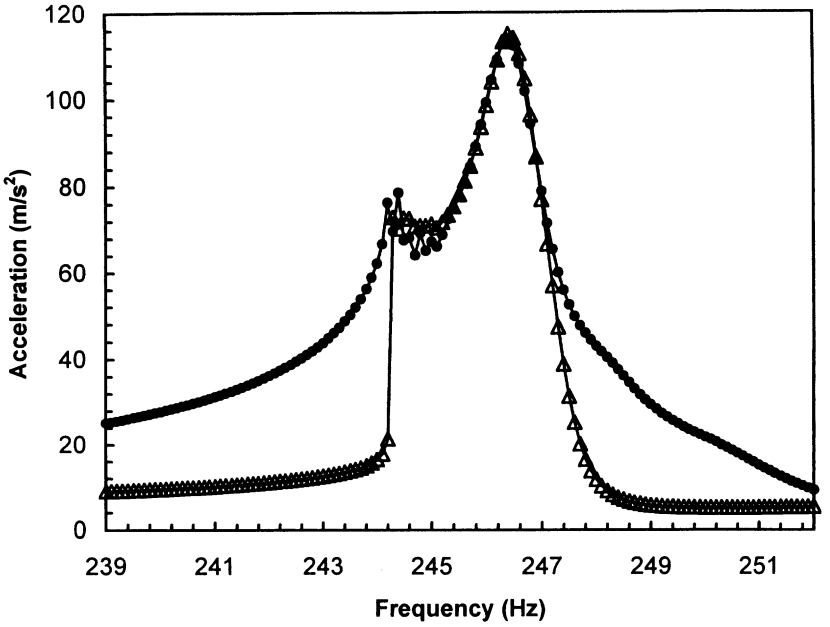

Fig. 32. Experimentally measured acceleration versus excitation frequency for modes ($n = 10, m = 1$) of the water-filled shell; force 3 N. —●—, 1st accelerometer; —△—, 2nd accelerometer.

a sinusoidal function of time and the measured accelerations are relatively small. Numerical calculations have been produced using the DIVPAG routine of IMSL, for time integration, to reproduce the system response and are plotted in Fig. 36. The Fourier series calculated from the experimental input force has been used to perform numerical simulations. In this case, the Fourier series follows closely a harmonic function. The series is given by equation (D.1) in Appendix D. Modes with eight circumferential waves have also been used in the mode expansion because the natural frequency of mode ($n = 8$, $m = 1$) is almost twice the natural frequency of the fundamental mode; for this reason mode ($n = 8$, $m = 1$) is excited by harmonics of the force excitation that are always present in experimental tests (they are generally small at a distance from resonance, but they can become important when frequency is close to resonance) and could have an interaction with the fundamental mode. In particular, modes with 5, 8, 10 and 16 circumferential waves have been used in the expansion in addition to four axisymmetric modes. The calculated accelerations at the two locations of the accelerometers have been obtained by using all the generalized co-ordinates introduced in the expansion. The agreement between numerical and experimental results is strong.

The experimental force input and accelerations for the fundamental mode ($n = 5, m = 1$) of the water-filled shell are shown in Fig. 37 versus time for excitation of magnitude 3 N and frequency 75.525 Hz measured by decreasing the excitation frequency (down). In these conditions, the shell response is the one obtained very close to the peak in Fig. 22(b) for force of 3 N. The input force is no more a pure sinusoidal function of time and the measured accelerations are quite large. For acceleration very close to the peak, the corresponding input force has been found to be similarly distorted for forces of 3 N or larger. However, moving little away from the peak, the force

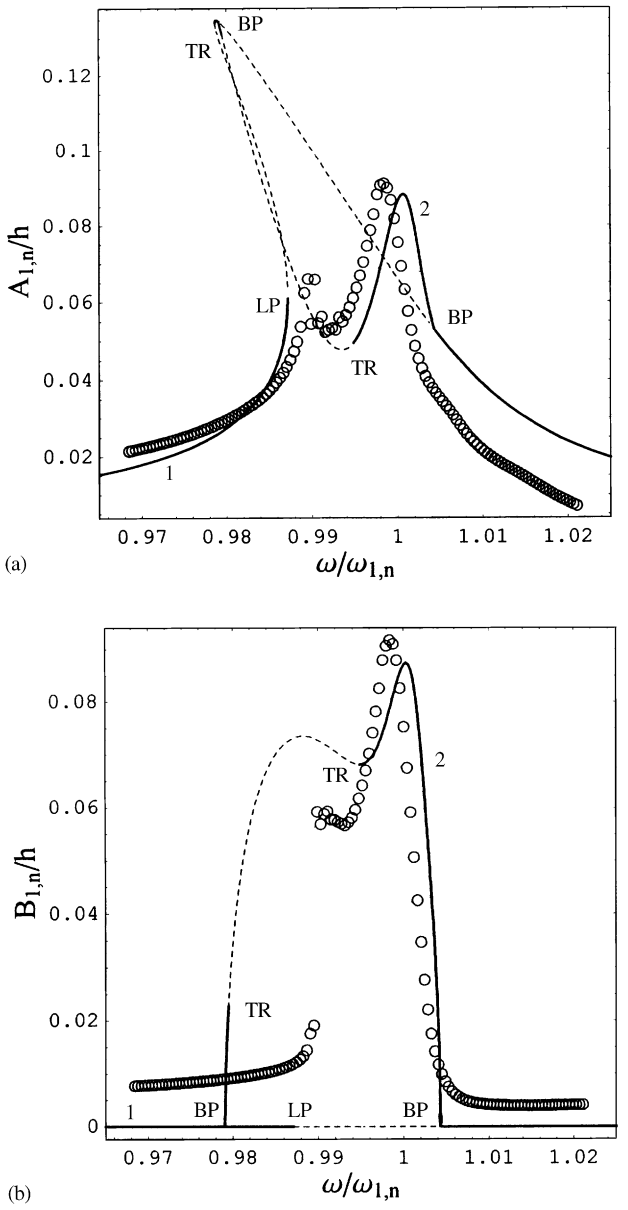

Fig. 33. Response amplitude–frequency relationship for mode ($n = 10$, $m = 1$) of the water-filled shell; force 3 N. ○, experimental data; ——, stable theoretical solutions; – – –, unstable theoretical solutions. (a) displacement/h from the 1st accelerometer; (b) displacement/h from the 2nd accelerometer. 1, branch "1"; 2, branch "2"; BP, pitchfork bifurcation; TR, Neimark–Sacker bifurcations; LP, limit point.

behaviour is more similar to a simple harmonic function, as shown in Fig. 35(a). In this case a travelling wave response around the shell is observed and the phase shift between the first and second accelerometer is about $\pi/2$. Numerical calculations are given in Fig. 38. The Fourier series calculated from the experimental input force, see Eq. (D.2) in Appendix D, has been used to

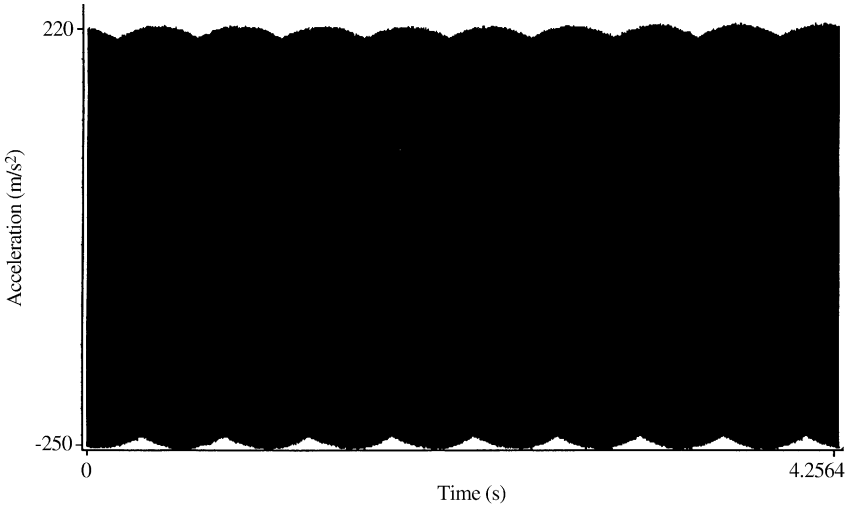

Fig. 34. Time response of the 1st accelerometer for mode ($n = 10$, $m = 1$) of the water-filled shell; force 14 N, frequency 240.5 Hz.

perform numerical calculations. Contribution of all modes has been used to evaluate the accelerations at the locations of the two sensors. Modes with eight circumferential waves have also been used in the mode expansion. The agreement between numerical and experimental results is quite good. Fig. 39 presents the same calculations obtained by using a mode expansion that does not include mode ($n = 8$, $m = 1$). In this case the numerical response does not contain some harmonics associated with vibrations of mode shape ($n = 8$, $m = 1$). The corresponding theoretical results for this specific case are in less agreement with experimental data. This weak agreement between the theoretical and experimental results shows that asymmetric modes with different number of circumferential waves with respect to the resonant mode should be included in the mode expansion if they have a 1:1, 1:2 or 1:3 relationships with the frequency of the resonant mode.

For all the modes considered, generally the shell response is much closer to a simple harmonic response than the one given in Fig. 37, also in case of distorted input. In fact, this is a particularly distorted response due to participation of mode ($n = 8, m = 1$) excited by the 2nd harmonic of the force excitation.

9. Conclusions

Numerical simulations and experiments on a steel shell, both empty and water-filled, show good agreement for the different modes investigated and for different magnitudes of harmonic excitation forces. This indicates that Donnell's non-linear shallow-shell theory gives accurate results within the limit of applicability of the theory, i.e., very thin shells, vibration amplitude of the order of the shell thickness and number of circumferential waves larger than four. Geometric imperfections, mainly due to the longitudinal weld in the test shell, have been included in the

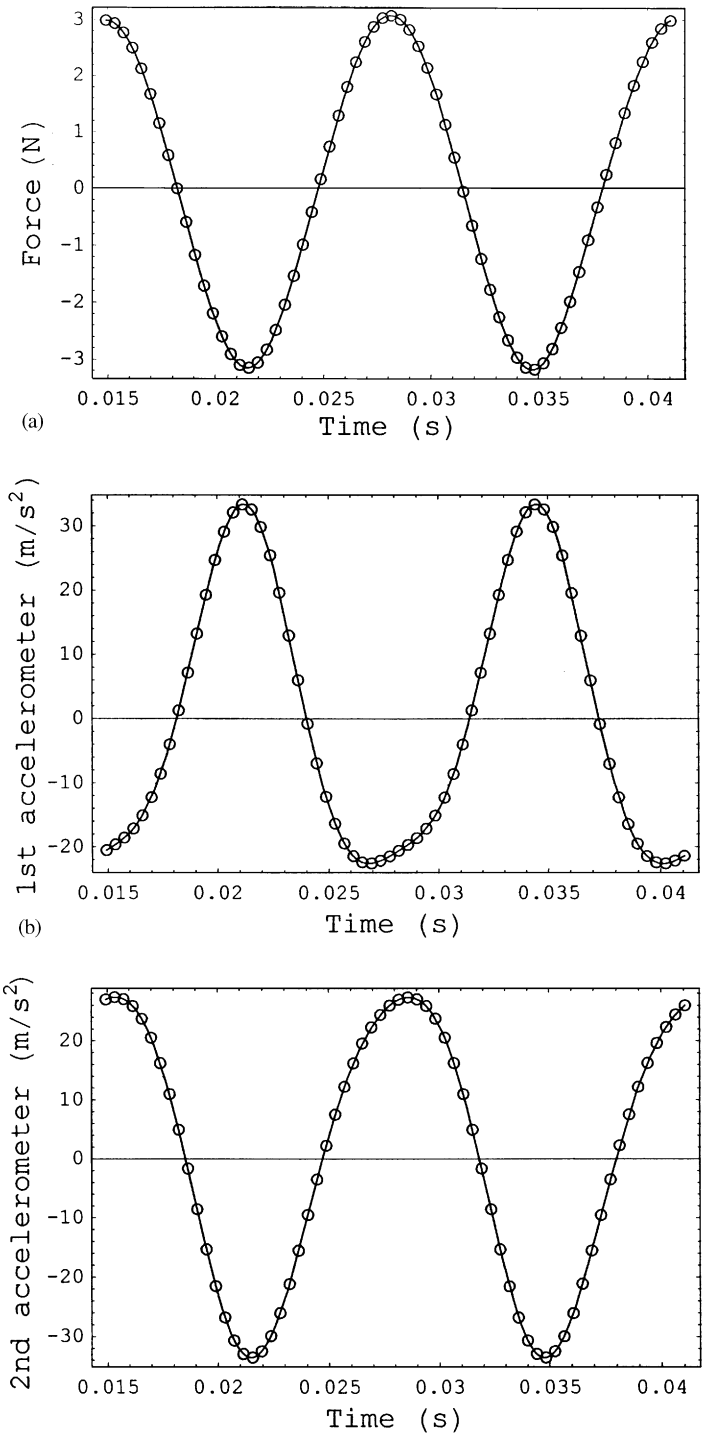

Fig. 35. Measured force and acceleration versus time for mode ($n = 5$, $m = 1$) of the water-filled shell; force 3 N, frequency 75.375 Hz down. ○, experimental data; ——, Fourier interpolation. (a) Excitation force; (b) 1st accelerometer; (c) 2nd accelerometer.

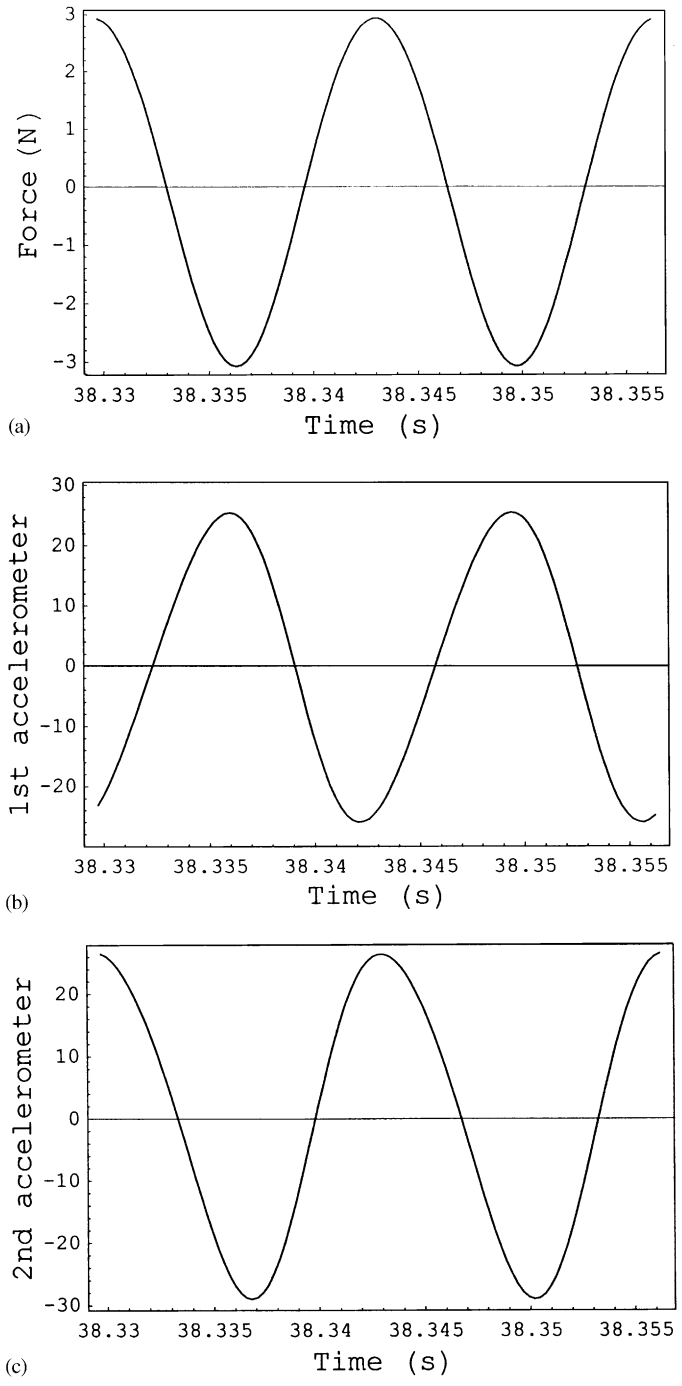

Fig. 36. Force input used in the model and calculated acceleration versus time for mode ($n = 5$, $m = 1$) of the water-filled shell; force 3 N, frequency 75.375 Hz down: (a) excitation force; (b) 1st accelerometer; (c) 2nd accelerometer.

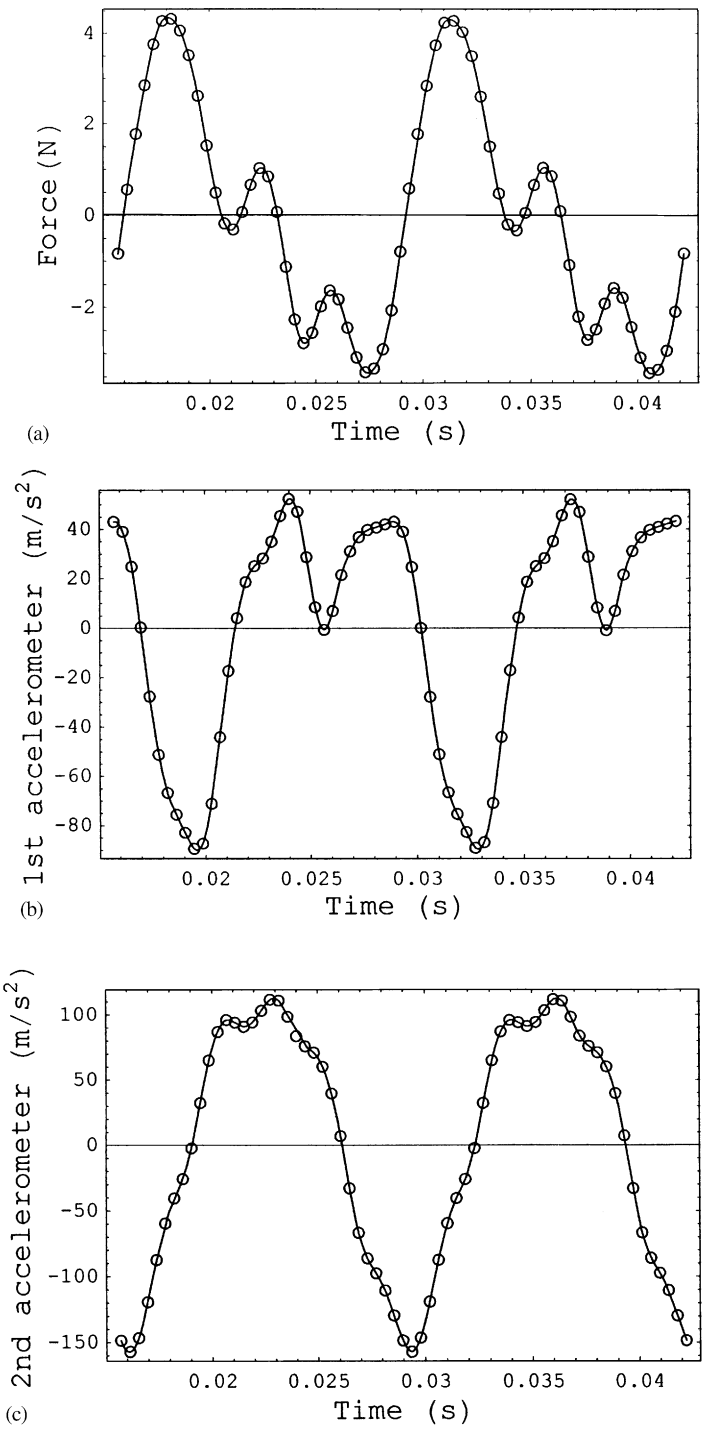

Fig. 37. Measured force and acceleration versus time for mode ($n = 5$, $m = 1$) of the water-filled shell; force 3 N, frequency 75.525 Hz down. ○, experimental data; ——, Fourier interpolation. (a) Excitation force; (b) 1st accelerometer; (c) 2nd accelerometer.

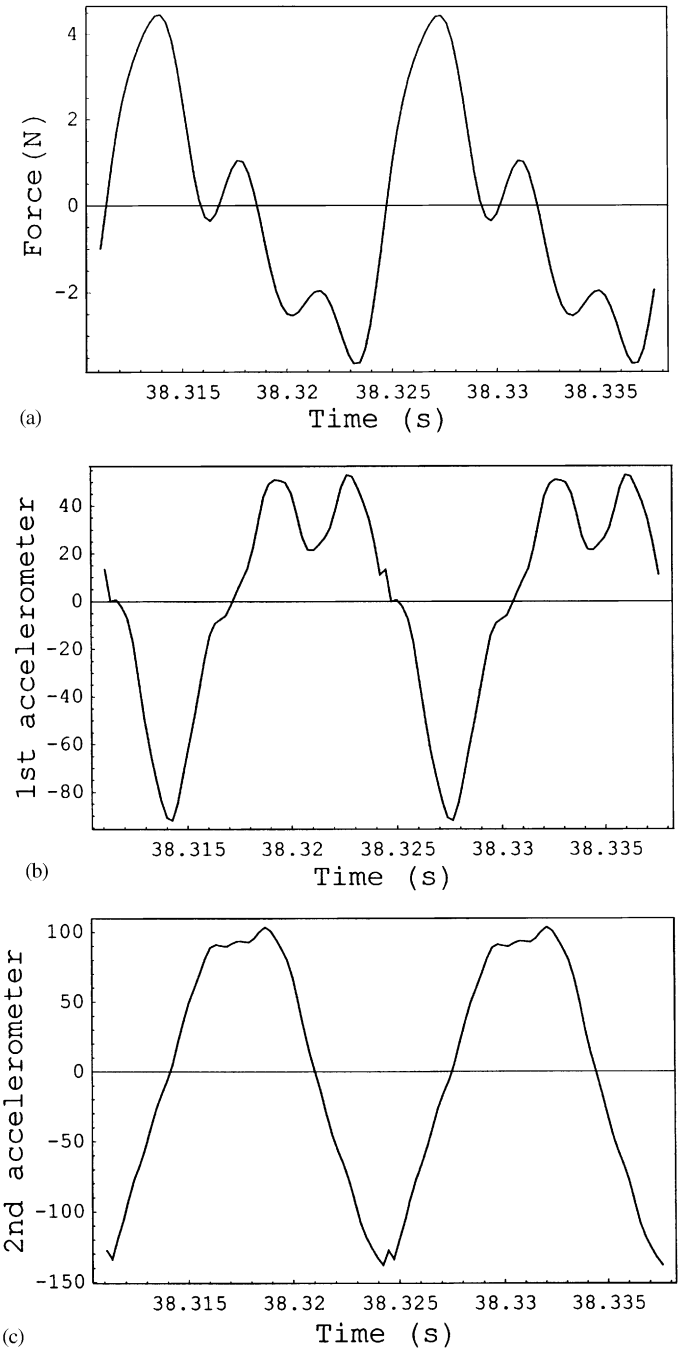

Fig. 38. Force input used in the model and calculated acceleration versus time for mode ($n = 5$, $m = 1$) of the water-filled shell; force 3 N, frequency 75.525 Hz down: (a) excitation force; (b) 1st accelerometer; (c) 2nd accelerometer.

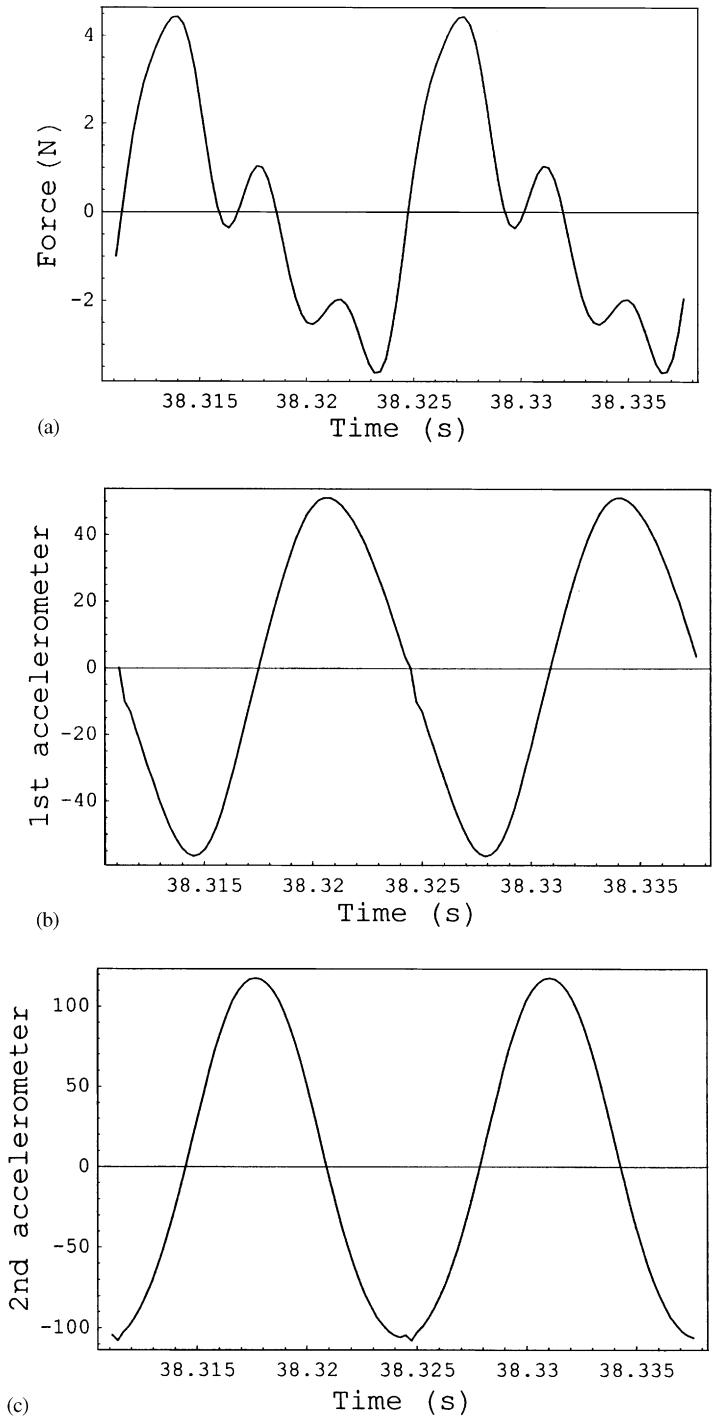

Fig. 39. Force input used in the model and calculated acceleration versus time for mode ($n = 5$, $m = 1$) of the water-filled shell neglecting participation of mode ($n = 8$, $m = 1$); force 3 N, frequency 75.525 Hz down: (a) excitation force; (b) 1st accelerometer; (c) 2nd accelerometer.

model and have been used to reproduce with accuracy the split of natural frequencies associated with each asymmetric mode. Measured geometric imperfections, detected from Fourier analysis of samples taken on limited number of circumferences, are in reasonable agreement with the values needed to reproduce the natural frequencies. Imperfections with $2n$ circumferential waves are those that give the largest effect on natural frequency for the mode with n circumferential waves.

The split of the double eigenvalue, due to imperfections in the test shell, alters the non-linear behaviour fundamentally. In particular, five types of different non-linear behaviours have been identified experimentally and simulated numerically: (i) softening-type non-linearity with bifurcation of the driven mode response and appearance of travelling wave, characteristics of shell without imperfections (mode $n = 10$, $m = 1$, water-filled shell); (ii) softening-type non-linearity without bifurcation of the driven mode and with appearance of travelling wave, characteristics of shell with small split of the double eigenvalue (modes $n = 5$ and $n = 7$, $m = 1$, water-filled shell); (iii) softening-type non-linearity without bifurcation and no travelling wave response, characteristics of relatively large split of the double eigenvalue (modes $n = 5m = 1$, empty shell); (iv) interaction of asymmetric modes with different number of circumferential waves that happens when they have very close natural frequencies; no change of the resonance frequency is observed with increasing vibration amplitude (modes $n = 4$ and 6, $m = 1$, water-filled shell); (v) amplitude-modulated response around resonance, through Neimark–Sacker bifurcation of the travelling wave response, characteristics of modes with significant softening non-linearity and almost without split of the double eigenvalue (mode $n = 10$, $m = 1$, water-filled shell).

The non-linear softening behaviour of the shell is largely increased by filling it with water. The softening behaviour helps the formation of travelling wave response around the shell. This travelling response appears also for relatively small vibration amplitudes, smaller than $\frac{1}{10}$ of the shell thickness. In particular, travelling wave response always appears for sufficiently large excitation when the double eigenvalue associated to asymmetric modes is not split or it is split in two different frequencies with values very close to each other.

The identified modal damping increases with the magnitude of the harmonic excitation force. This change is almost linear if there is no travelling wave around the shell circumference; otherwise the relationship between damping and force is strongly non-linear.

Acknowledgements

This work was partially supported by the COFIN 2000 grant of the Italian Ministry for University and Research (MURST). I would like to thank Professors M.P. Païdoussis and F. Pellicano who have worked with me on several problems of non-linear dynamics of shell structures. Ing. F. Pagnanelli, Ing. M. Pellegrini and Ing. D. Rabotti are thanked for helping me with the experiments. M. Eng. K. Karagiozis is thanked for proofreading the manuscript. The present paper is dedicated to the 70th birthday of my beloved father, Dr. Vito Amabili, and to the late "zia-nonna" Luigia Copetti.

Appendix A. Particular solution of the stress function

The technique used to calculate the functions of time F_{mnj}, $j = 1, \ldots, 4$, in Eq. (23) by using the *Mathematica* computer program [28] for symbolic manipulations is described here. If Eq. (11a) is substituted into the right-hand side of Eq. (3), after some algebra the following expressions are obtained:

$$\frac{1}{R}\frac{\partial^2 w}{\partial x^2} = \frac{\pi^2}{RL^2}\frac{\partial^2 w}{\partial \eta^2} = -\frac{\pi^2}{RL^2}\sum_{m=1}^{M}\sum_{n=0}^{N}(A_{mn}\cos n\theta + B_{mn}\sin n\theta)m^2 \sin m\eta, \tag{A.1}$$

$$\left(\frac{1}{R}\frac{\partial^2 w}{\partial x \partial \theta}\right)^2 = \frac{\pi^2}{R^2L^2}\sum_{m_1=1}^{M}\sum_{m_2=1}^{M}\sum_{n_1=0}^{N}\sum_{n_2=0}^{N} m_1 m_2 n_1 n_2 \cos m_1\eta \cos m_2\eta(-A_{m_1n_1}\sin n_1\theta + B_{m_1n_1}\cos n_1\theta)(-A_{m_2n_2}\sin n_2\theta + B_{m_2n_2}\cos n_2\theta), \tag{A.2}$$

$$\frac{\partial^2 w}{\partial x^2}\frac{\partial^2 w}{R^2\partial\theta^2} = \frac{\pi^2}{R^2L^2}\sum_{m_1=1}^{M}\sum_{m_2=1}^{M}\sum_{n_1=0}^{N}\sum_{n_2=0}^{N} m_1^2 n_2^2 \sin m_1\eta \sin m_2\eta(A_{m_1n_1}\cos n_1\theta + B_{m_1n_1}\sin n_1\theta) \times (A_{m_2n_2}\cos n_2\theta + B_{m_2n_2}\sin n_2\theta), \tag{A.3}$$

$$\frac{2\partial^2 w}{R\partial x\partial\theta}\frac{\partial^2 w_0}{R\partial x\partial\theta} = \frac{2\pi^2}{R^2L^2}\sum_{m_1=1}^{M}\sum_{m_2=1}^{\tilde{M}}\sum_{n_1=0}^{N}\sum_{n_2=0}^{\tilde{N}} m_1 m_2 n_1 n_2 \cos m_1\eta \cos m_2\eta(-A_{m_1n_1}\sin n_1\theta + B_{m_1n_1}\cos n_1\theta)(-\tilde{A}_{m_2n_2}\sin n_2\theta + \tilde{B}_{m_2n_2}\cos n_2\theta), \tag{A.4}$$

$$-\left(\frac{\partial^2 w}{\partial x^2}\frac{\partial^2 w_0}{R^2\partial\theta^2} + \frac{\partial^2 w_0}{\partial x^2}\frac{\partial^2 w}{R^2\partial\theta^2}\right) = \frac{-\pi^2}{R^2L^2}\sum_{m_1=1}^{M}\sum_{m_2=1}^{\tilde{M}}\sum_{n_1=0}^{N}\sum_{n_2=0}^{\tilde{N}}(m_1^2n_2^2 + m_2^2n_1^2)\sin m_1\eta \sin m_2\eta \times (A_{m_1n_1}\cos n_1\theta + B_{m_1n_1}\sin n_1\theta)(\tilde{A}_{m_2n_2}\cos n_2\theta + \tilde{B}_{m_2n_2}\sin n_2\theta), \tag{A.5}$$

where N is the same as in Eq. (11a), M is the largest between M_1 and M_2, $\tilde{M}$ is the largest between $\tilde{M}_1$ and $\tilde{M}_2$ and $\eta = \pi x/L$; the time dependence has been suppressed here for sake of brevity. By substituting Eqs. (A.1)–(A.5) and (23) into Eq. (3), the unknown functions F_{mni} can be identified by using the computer program *Mathematica* 4 [28].

Appendix B. Average in-plane restraint stresses

According with the boundary conditions (8) and (9) it is assumed that

$$\bar{N}_x = \text{constant (in particular, } \bar{N}_x = 0), \qquad \bar{N}_{x\theta} = 0. \tag{B.1}$$

As a consequence, after simple calculations it is obtained that

$$\bar{N}_\theta = \nu \bar{N}_x + \frac{Eh}{2\pi RL}\int_0^{2\pi}\int_0^{L}\left[-\frac{w}{R}+\tfrac{1}{2}\left(\frac{\partial w}{R\partial\theta}\right)^2+\frac{\partial w}{R\partial\theta}\frac{\partial w_0}{R\partial\theta}\right]\mathrm{d}x R\,\mathrm{d}\theta. \tag{B.2}$$

By inserting Eqs. (11a) and (12) into Eq. (B.2), the following expression is obtained:

$$\bar{N}_\theta = \nu \bar{N}_x + \frac{Eh}{2\pi R}\left\{-2\sum_{m=1}^{M_2}\frac{A_{m,0}(t)}{m}[1-(-1)^m]+\frac{\pi}{4R}\sum_{n=1}^{N}\sum_{m=1}^{M_1} n^2(A_{m,n}^2(t)+B_{m,n}^2(t)) + \frac{\pi}{2R}\sum_{n=1}^{\bar{N}}\sum_{m=1}^{\bar{M}} n^2(\tilde{A}_{m,n}A_{m,n}(t)+\tilde{B}_{m,n}B_{m,n}(t))\right\}, \tag{B.3}$$

where $\bar{N}$ is the smallest between N and $\tilde{N}$ and $\bar{M}$ is the smallest between M_1 and $\tilde{M}_1$.

Appendix C. Data on geometric imperfections

The following Fourier series describes geometric imperfections on the central circumference of the test shell, where terms with more than 20 waves have been neglected. The coefficients of the series are given in millimeters/100:

$$\begin{aligned}&26.35\cos(2\theta)-4.00\cos(3\theta)-0.75\cos(4\theta)-0.43\cos(5\theta)+6.51\cos(6\theta)\\&+3.54\cos(7\theta)-7.94\cos(8\theta)-9.83\cos(9\theta)-0.06\cos(10\theta)+4.99\cos(11\theta)+4.52\cos(12\theta)\\&-0.77\cos(13\theta)-5.04\cos(14\theta)-3.74\cos(15\theta)+1.48\cos(16\theta)+4.87\cos(17\theta)+2.90\cos(18\theta)\\&-2.02\cos(19\theta)-4.51\cos(20\theta)+31.40\sin(2\theta)+6.57\sin(3\theta)-3.78\sin(4\theta)\\&+4.19\sin(5\theta)-5.83\sin(6\theta)-1.66\sin(7\theta)+9.60\sin(8\theta)-1.22\sin(9\theta)-5.73\sin(10\theta)\\&-2.62\sin(11\theta)+3.20\sin(12\theta)+5.38\sin(13\theta)+1.72\sin(14\theta)-3.62\sin(15\theta)-4.86\sin(16\theta)\\&-0.86\sin(17\theta)+3.83\sin(18\theta)+4.20\sin(19\theta)+0.10\sin(20\theta).\end{aligned}$$

The normalized amplitudes of imperfections with 5, 10, 12, 14 and 20 circumferential waves are therefore $0.081h$, $0.11h$, $0.107h$, $0.103h$ and $0.087h$, respectively.

Appendix D. Data on measured input forces

The time series obtained by Fourier analysis of the periodic force input of harmonic magnitude of 3 N and frequency 75.375 Hz down is

$$3.06\cos(\omega t)-0.68\cos(2\omega t)+0.023\cos(3\omega t)+0.013\cos(4\omega t)+\cdots. \tag{D.1}$$

The time series obtained by Fourier analysis of the periodic force input of harmonic magnitude of 3 N and frequency 75.525 Hz down is

$$\begin{aligned}&2.94\sin(\omega t)+1.29\sin(2\omega t)-0.37\cos(2\omega t)+0.2\sin(3\omega t)-0.87\cos(3\omega t)\\&+0.25\sin(4\omega t)+0.52\cos(4\omega t)+0.15\sin(5\omega t)+0.08\cos(5\omega t)+\cdots.\end{aligned} \tag{D.2}$$

References

[1] M. Amabili, M.P. Païdoussis, Review of studies on geometrically nonlinear vibrations and dynamics of circular cylindrical shells and panels, with and without fluid–structure interaction, Applied Mechanics Reviews, in press.

[2] D.A. Evensen, Nonlinear flexural vibrations of thin-walled circular cylinders. NASA TN D-4090, 1967.

[3] E.H. Dowell, C.S. Ventres, Modal equations for the nonlinear flexural vibrations of a cylindrical shell, International Journal of Solids and Structures 4 (1968) 975–991.

[4] J.H. Ginsberg, Large amplitude forced vibrations of simply supported thin cylindrical shells, Journal of Applied Mechanics 40 (1973) 471–477.

[5] J.C. Chen, C.D. Babcock, Nonlinear vibration of cylindrical shells, American Institute of Aeronautics and Astronautics Journal 13 (1975) 868–876.

[6] M. Ganapathi, T.K. Varadan, Large amplitude vibrations of circular cylindrical shells, Journal of Sound and Vibration 192 (1996) 1–14.

[7] P.B. Gonçalves, R.C. Batista, Non-linear vibration analysis of fluid-filled cylindrical shells, Journal of Sound and Vibration 127 (1988) 133–143.

[8] M. Amabili, F. Pellicano, M.P. Païdoussis, Nonlinear vibrations of simply supported, circular cylindrical shells, coupled to quiescent fluid, Journal of Fluids and Structures 12 (1998) 883–918.

[9] M. Amabili, F. Pellicano, M.P. Païdoussis, Non-linear dynamics and stability of circular cylindrical shells containing flowing fluid. Part I: stability, Journal of Sound and Vibration 225 (1999) 655–699.

[10] M. Amabili, F. Pellicano, M.P. Païdoussis, Non-linear dynamics and stability of circular cylindrical shells containing flowing fluid. Part II: large-amplitude vibrations without flow, Journal of Sound and Vibration 228 (1999) 1103–1124.

[11] M. Amabili, F. Pellicano, M.P. Païdoussis, Non-linear dynamics and stability of circular cylindrical shells containing flowing fluid. Part III: truncation effect without flow and experiments, Journal of Sound and Vibration 237 (2000) 617–640.

[12] M. Amabili, F. Pellicano, M.P. Païdoussis, Non-linear dynamics and stability of circular cylindrical shells containing flowing fluid. Part IV: large-amplitude vibrations with flow, Journal of Sound and Vibration 237 (2000) 641–666.

[13] M. Amabili, F. Pellicano, M.P. Païdoussis, Nonlinear stability of circular cylindrical shells in annular and unbounded axial flow, Journal of Applied Mechanics 68 (2001) 827–834.

[14] F. Pellicano, M. Amabili, M.P. Païdoussis, Effect of the geometry on the non-linear vibration of circular cylindrical shells, International Journal of Non-Linear Mechanics 37 (2002) 1181–1198.

[15] A.S. Vol'mir, Nonlinear Dynamics of Plates and Shells, Nauka, Moscow, 1972 (in Russian).

[16] V.D. Kubenko, P.S. Koval'chuk, T.S. Krasnopol'skaya, Effect of initial camber on natural nonlinear vibrations of cylindrical shells, Soviet Applied Mechanics 18 (1982) 34–39.

[17] L. Watawala, W.A. Nash, Influence of initial geometric imperfections on vibrations of thin circular cylindrical shells, Computers and Structures 16 (1983) 125–130.

[18] M. Amabili, F. Pellicano, Multi-mode approach to nonlinear supersonic flutter of imperfect circular cylindrical shells, Journal of Applied Mechanics 69 (2002) 117–129.

[19] V.F. Sivak, A.I. Telalov, Experimental investigation of vibrations of a cylindrical shell in contact with a liquid, Soviet Applied Mechanics 27 (1991) 484–488.

[20] M. Chiba, Non-linear hydroelastic vibration of a cantilever cylindrical tank. I. Experiment (Empty case), International Journal of Non-Linear Mechanics 28 (1993) 591–599.

[21] M. Chiba, Non-linear hydroelastic vibration of a cantilever cylindrical tank. II. Experiment (Liquid-filled case), International Journal of Non-Linear Mechanics 28 (1993) 601–612.

[22] M. Chiba, Experimental studies on a nonlinear hydroelastic vibration of a clamped cylindrical tank partially filled with liquid, American Society of Mechanical Engineers, Journal of Pressure Vessel Technology 115 (1993) 381–388.

[23] M. Amabili, R. Garziera, A. Negri, Experimental study on large-amplitude vibrations of water-filled circular cylindrical shells, Journal of Fluids and Structures 16 (2002) 213–227.

[24] M. Amabili, F. Pellicano, A.F. Vakakis, Nonlinear vibrations and multiple resonances of fluid-filled, circular shells. Part 1: equations of motion and numerical results, American Society of Mechanical Engineers, Journal of Vibration and Acoustics 122 (2000) 346–354.
[25] F. Pellicano, M. Amabili, A.F. Vakakis, Nonlinear vibrations and multiple resonances of fluid-filled, circular shells, Part 2: perturbation analysis, American Society of Mechanical Engineers, Journal of Vibration and Acoustics 122 (2000) 355–364.
[26] V.D. Kubenko, P.S. Koval'chuk, Problems of nonlinear multiple-mode vibrations of thin elastic shells of revolution, Proceedings of the Symposium on Nonlinear Dynamics of Shells and Plates, American Society of Mechanical Engineers International Mechanical Engineering Congress and Exposition (AMD Vol. 238), Orlando, USA, 2000, pp. 147–153.
[27] A.A. Lakis, A. Laveau, Non-linear dynamic analysis of anisotropic cylindrical shells containing a flowing fluid, International Journal of Solids and Structures 28 (1991) 1079–1094.
[28] S. Wolfram, The Mathematica Book, 4th Edition, Cambridge University Press, Cambridge, UK, 1999.
[29] E.J. Doedel, A.R. Champneys, T.F. Fairgrieve, Y.A. Kuznetsov, B. Sandstede, X. Wang, AUTO 97: Continuation and Bifurcation Software for Ordinary Differential Equations (with HomCont),Concordia University, Montreal, Canada, 1998.
[30] M. Amabili, R. Garziera, Vibrations of circular cylindrical shells with nonuniform constraints, elastic bed and added mass; Part I: empty and fluid-filled shells, Journal of Fluids and Structures 14 (2000) 669–690.